Formation and decay of *isolated* anti-protonic atoms

R. Seki Osaka Univ., RCNP
in collaboration with members of PUMA group

Antiproton-nucleus interactions and related phenomena
ECT*- Trento, 17-21 June, 2019

Outline

1. The issue: (Decay of anti-protonic atoms)
   X-ray spectroscopy of anti-protonic atoms for nuclear physics
   (LEAR PS209 X-ray experiment)
2. Nature of atomic capture and atomic cascade.
   (Fermi-Teller model)
3. Atomic capture (Formation of anti-protonic atoms)
   (by light and heavy atoms)
4. Atomic cascade
   (LEAR PS175 X-ray experiment)
5. Prospects in the physics of anti-protonic atoms.
   (PUMA)

1. The issue: X-ray spectroscopy of anti-protonic atoms for nuclear physics

Overlap of the proton and neutron densities (in two parameter Fermi form) of ^{176}Yb
PS209 [TU Mùnich-Warsaw group at LEAR: R. Schmidt et al. *Phys. Rev.* **C58** 3195 (1998)]

A(n,ℓ) :
Anti-proton absorption distribution (r)
of the (n,ℓ) state
~ Overlap of [atomic densities (n, ℓ; r)
x anti-proton arrival prob. (n, ℓ)
x anti-proton absorption rate (n, ℓ)]
and [ρ(*p*) or ρ(*n*)]

Determined by
Atomic shift-widths data
and Atomic cascade computation
→ A(n,ℓ) and
[ρ(*p*) and ρ(*n*) parameters]

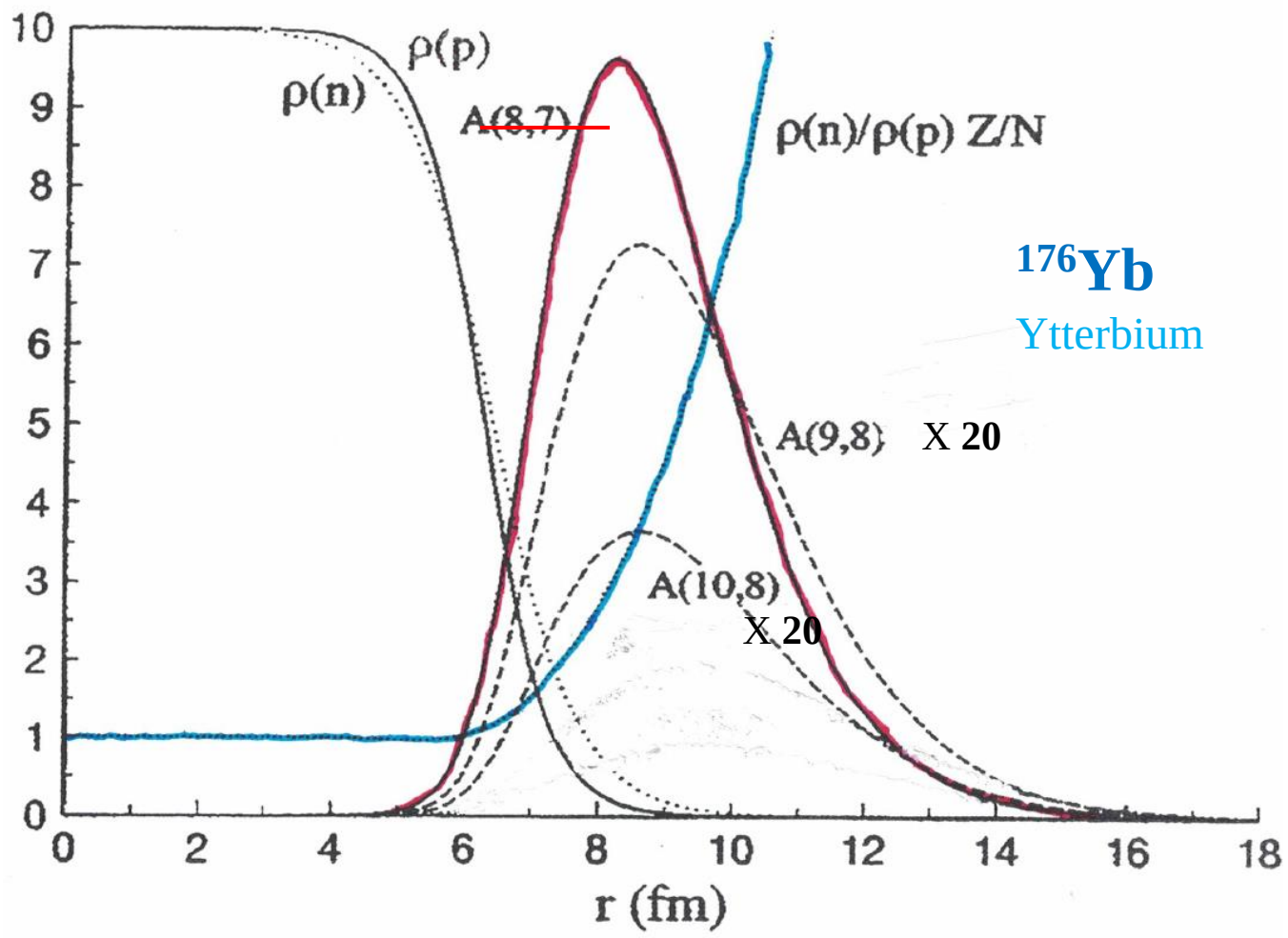

Atomic energy level transition schemescheme

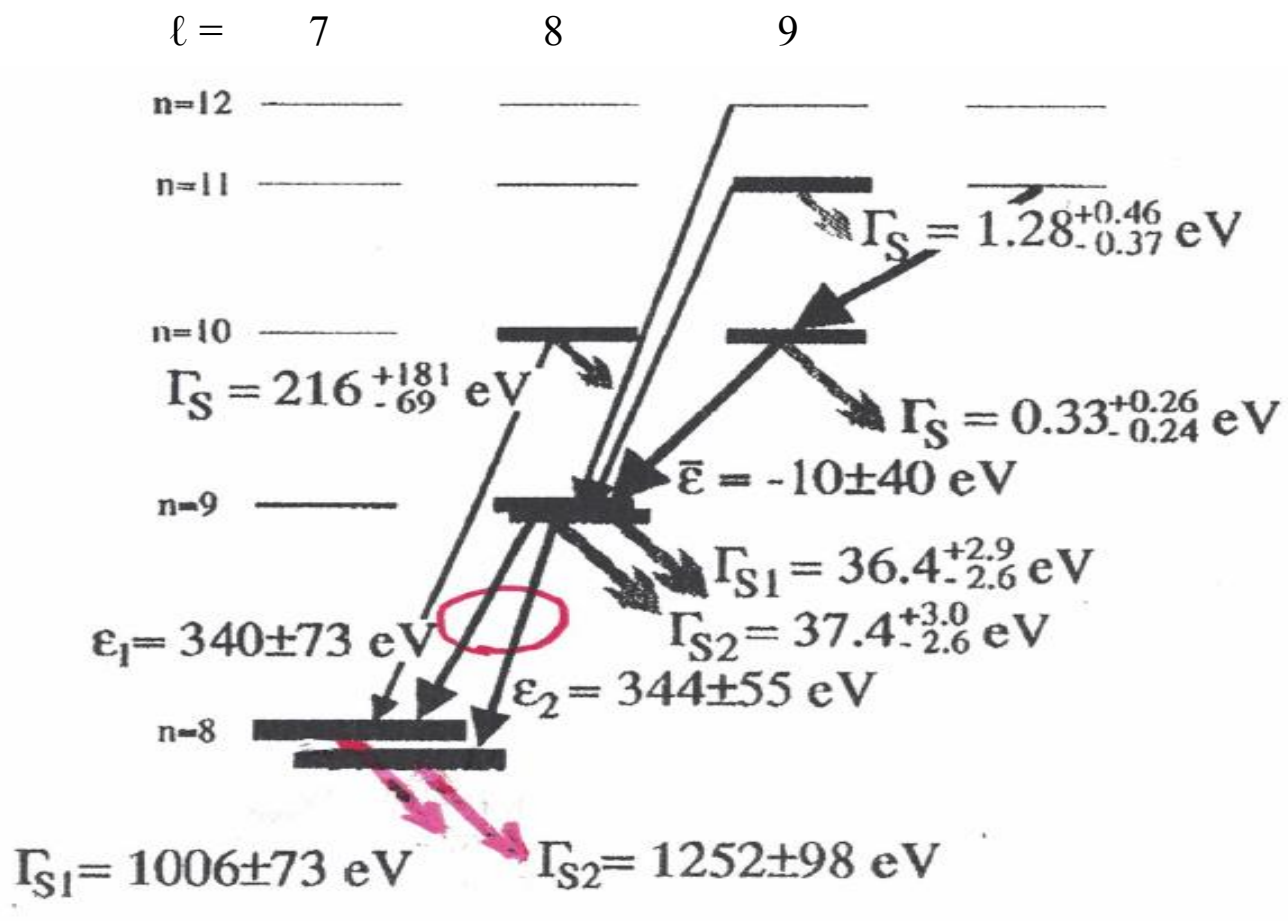

1. Nuclear absorption occurs from
(a) the upper energy levels (here, n=9) and
(b) the lower energy levels (here, n=8).

2. The last (most energetic) X-ray transition peak is (a) → (b); 9 → 8

3. The intensity of the last transition peak (relative-to-the previous peak) yields the absorption width of the upper level (b).
(N.B. the center-of-mass motion correction: the Fried-Martin factor)

R. Schmidt et al. (PS209) *Phys Rev*. **C58**, 195 (1998)

Cascade process viewed in PS209 X-ray spectrum

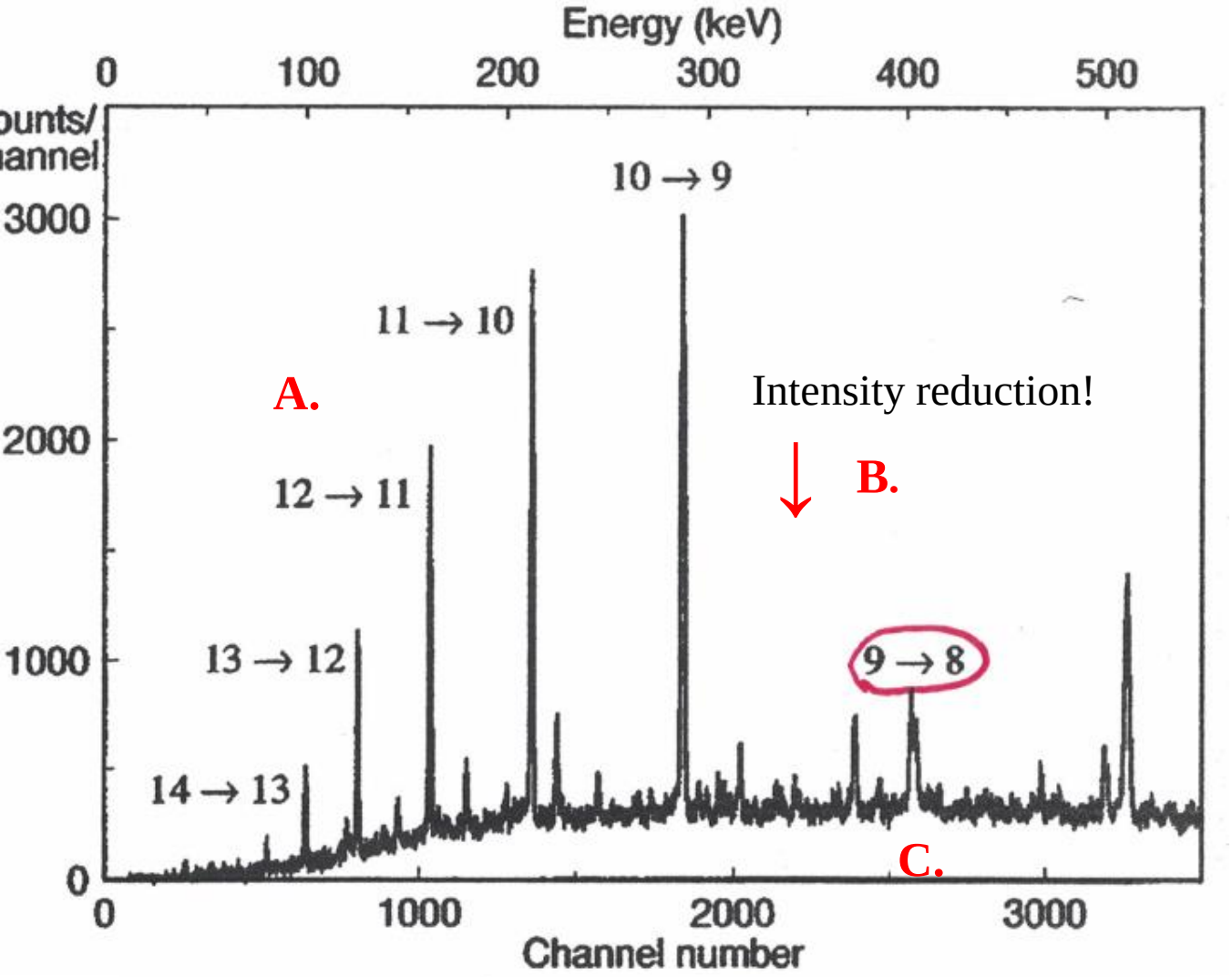

FIG. 2. Antiprotonic x-ray spectrum from ^{176}Yb measured with detector 2 (coaxial HPGe detector with an outer diameter of 49 mm and a length of 49.5 mm). One channel corresponds to 0.157 keV.

A. Up to $10 \rightarrow 9$, as n ↓,
intensity (count) and ΔE (Δchannel no) ↑.

B. But $I(9 \rightarrow 8) \ll I(10 \rightarrow 9)$
and no visible $I(8 \rightarrow 7)$

C. $I(9 \rightarrow 8)$ is broader than the other I's

↓

D. Ant-protons disappear from
n = 9 and
n = 8 atomic levels (states)

in competition to the radiative transitions.

R. Schmidt et al. (PS209) PRC 58(1998)3195

Extracted by PS209 and radiochemical experiment.

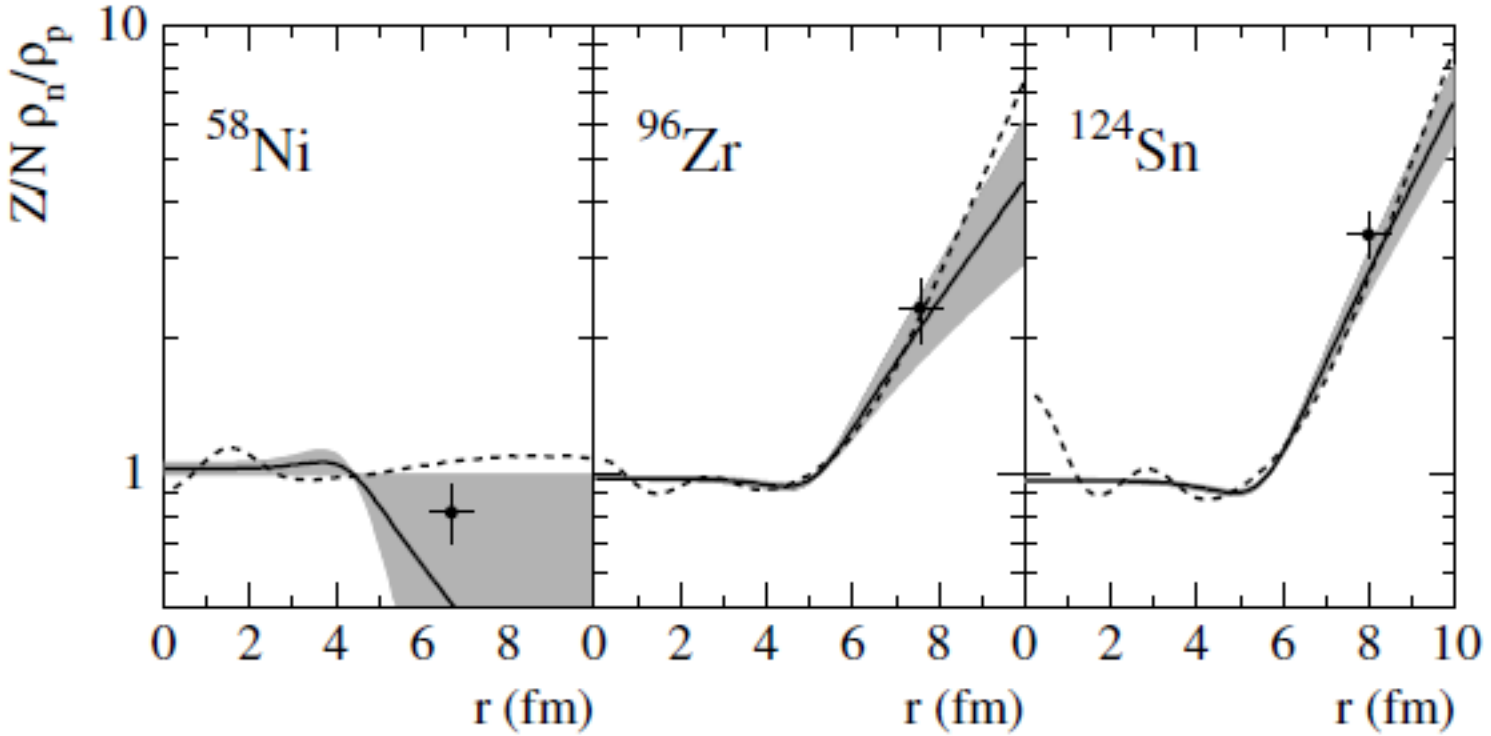

FIG. 2. Normalized neutron to proton density ratios $\frac{Z}{N}\frac{\rho_n}{\rho_p}$ deduced from strong-interaction level widths and shifts (solid lines with indicated statistical error) and charge distributions given in Refs. [38,41], for ^{58}Ni, ^{96}Zr, and ^{124}Sn, respectively. They are compared with f_{halo} measured in the radiochemical experiments (marked with crosses at a radial distance corresponding to the most probable annihilation site) and with HFB model calculations [40] (dashed lines).

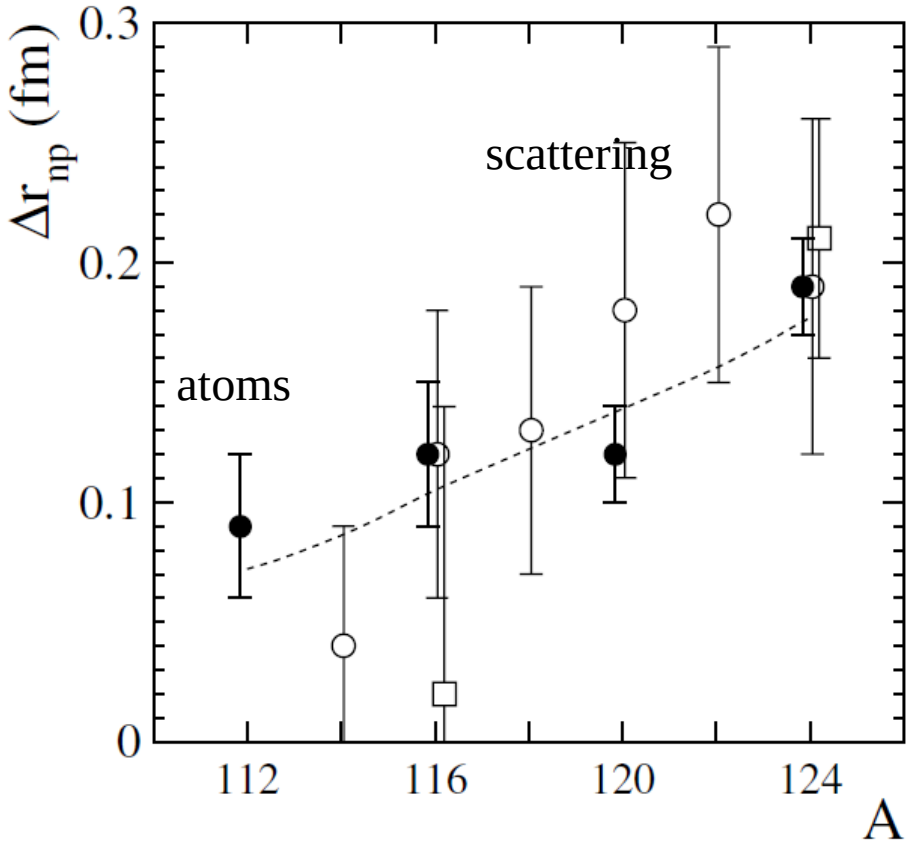

A. Trzcinska et al, *Phys. Rev. Lett* **87**, 082501 (2001)

Atomic cascade computation

$M_{\bar{p}} = 938.272 \text{ MeV and } m_e = 0.510999 \text{ MeV}$

$$\rightarrow \quad \sqrt{\frac{M_{\bar{p}}}{m_e}} \approx 42.85$$

$$B.E. = \frac{(Ze^2)^2 m}{2\hbar^2 n^2}$$

in Bohr atom

$$R = \frac{n^2\hbar^2}{Ze^2 m}$$

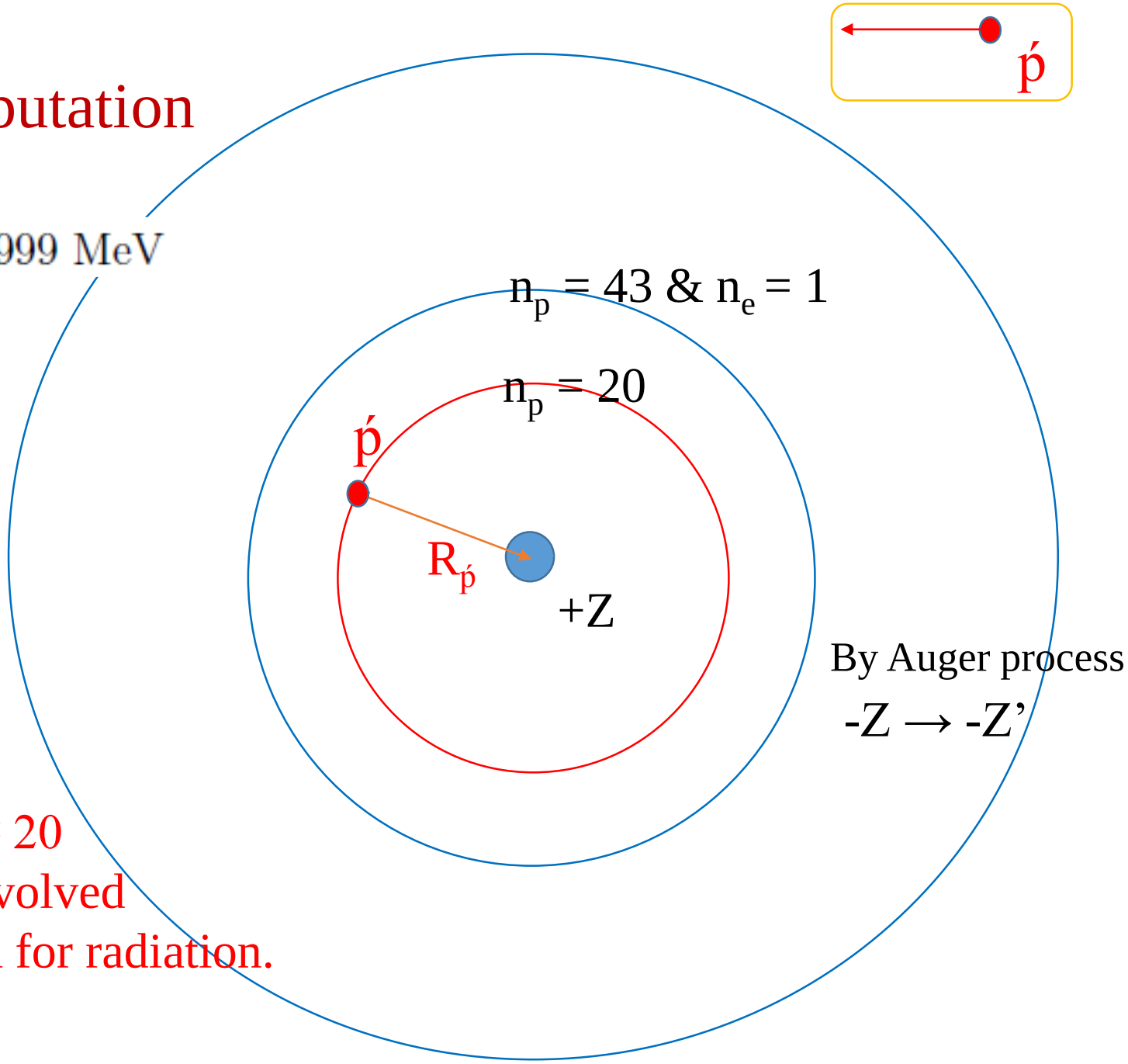

By Auger process

$-Z \rightarrow -Z'$

Cascade calculation starts at $n_p \approx 20$
because of less electron cloud involved
and of the dipole approx. applied for radiation.

Cascade scheme in exotic atoms

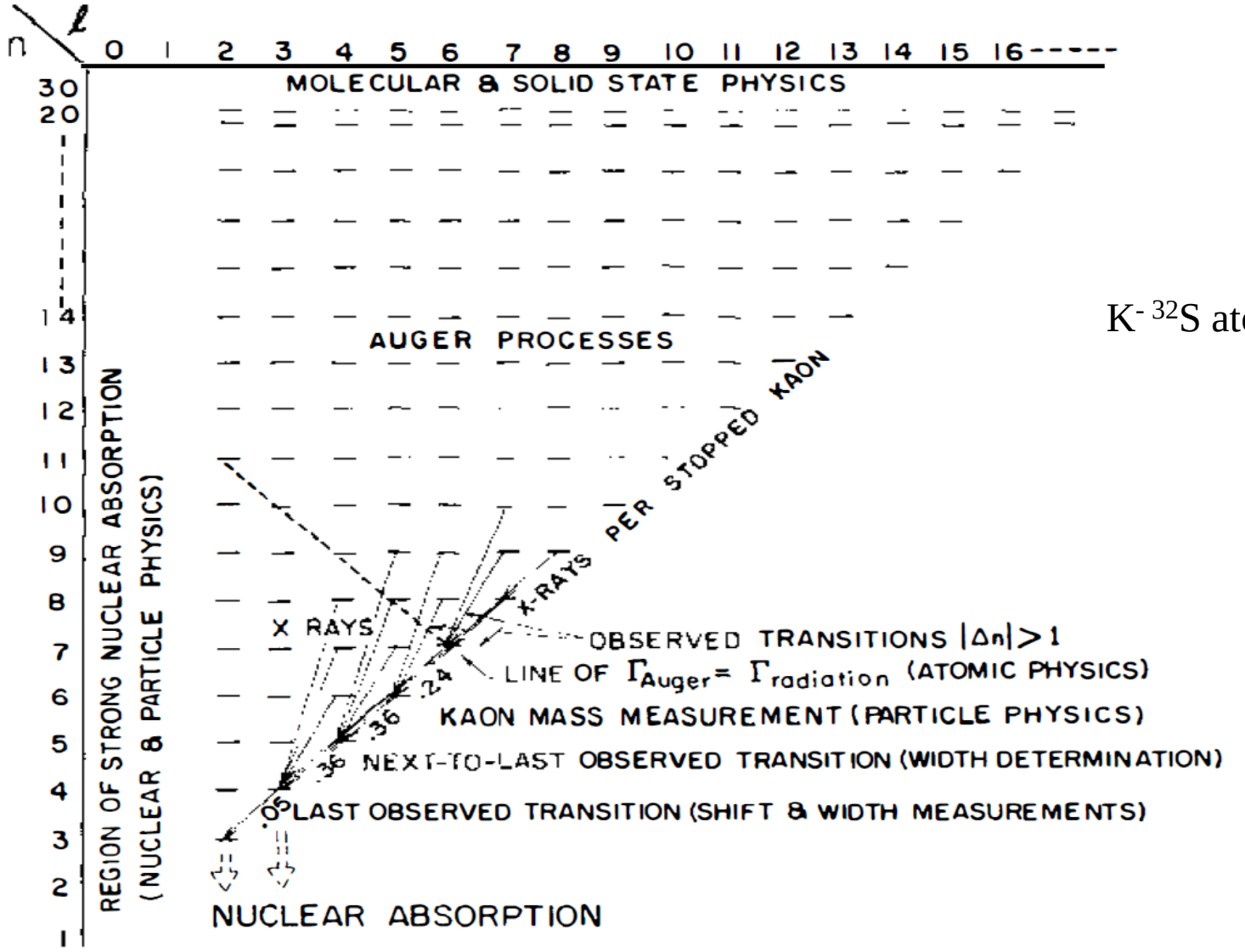

K$^-$ ^{32}S atom

Figure 7 Schematic diagram of kaonic $^{32}_{16}$S atoms showing some of the features of the cascade and nuclear absorption. The cascade was started at $n = 30$ where the angular momentum distribution of kaons was assumed to be proportional to $2l+1$ and l_{max} equaled $n-1$. Regions of applicability of various disciplines in physics are indicated.

Seki,Wiegand
Annu. Rev. Nucl. Sci.
25, 241(1975)

Needed information for cascade computation

1) The population distribution, $N(\ell)$ at n_p (≈ 20), at the start of the computation.

2) No. of Auger electrons at the start and during the computation, including Auger and electron refilling rates.

3) Widths and shifts of lower atomic levels, circular and noncircular. ← X-ray Data and their analysis

How 1) ~ 3) differ for isolated atoms?

Note: Current cascade-computation codes use the atomic structure information, effective charges of atoms associated with those of orbital electrons.

1) $N(\ell) = (2\ell + 1)\, e^{\alpha \ell}$

PS209 fits of α for isotopes (R. Schmidt, PhD thesis, TU Munich 1999)

Ca 0.129±0.019

Cd 0.101±0.014

Sn 0.169±0.008

α small: approximately statistical, with effects of electron depletion neglected.

But then in isolated atoms?

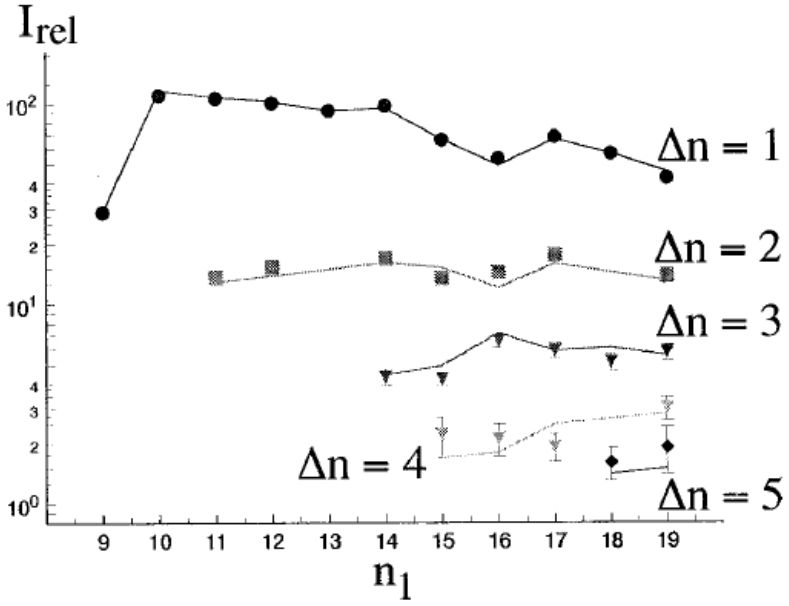

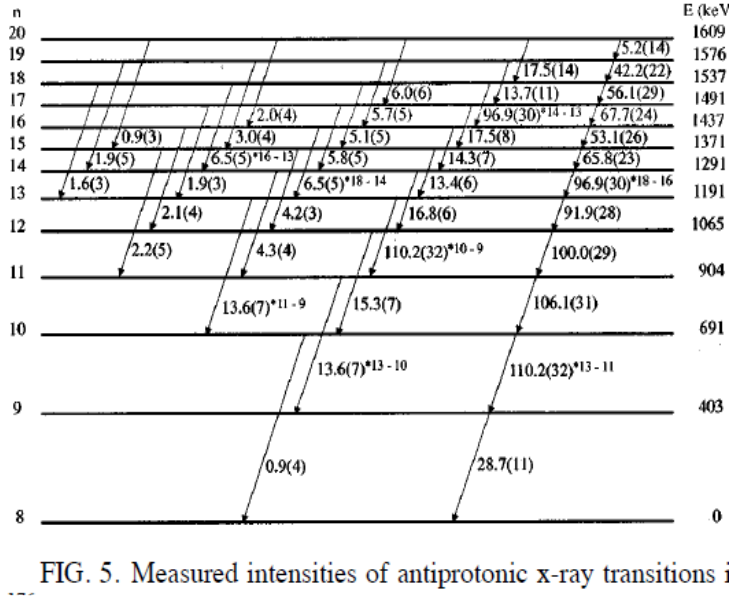

FIG. 5. Measured intensities of antiprotonic x-ray transitions i

R. Schmidt et. al (1998)

2) Auger electron information for isolated atoms

2. Nature of our problem on atomic capture and cascade

Atomic capture

Before

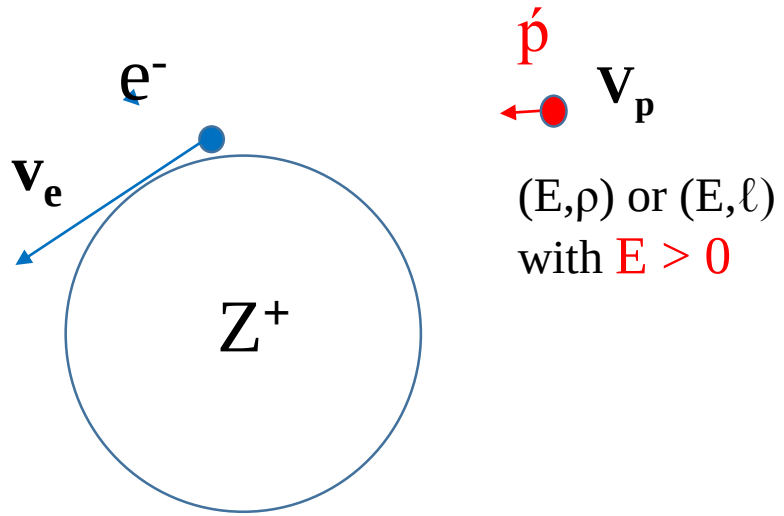

After

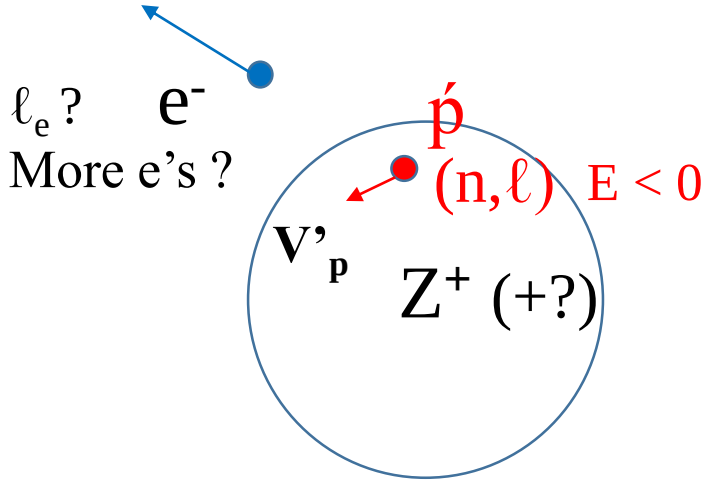

$V_p << v_e$

Adiabatic approx.
(~Born-Oppenheimer approx.):

Needed: Dependence on (n,ℓ) of "after" capture

A semi-classical statistical description of atomic capture and atomic cascade (through atomic electrons): Fermi-Teller model.

E. Fermi, E. Teller, *Phy. Rev*. **72**, 399 (1947).
M. Leon, R. Seki, *Nucl.Phys*.**A282** 445 (1977)*

Atomic capture

Energy loss by Auger electrons

$$-\frac{dW}{dt} = \int \frac{2d^3k_i}{(2\pi)^3} V_{rel} \Delta E \frac{d\sigma}{d\Omega_{cm}} d\Omega_{cm},$$

a) b) c) d)

a) Electron density in Thomas-Fermi gas
b) Relative velocity between e and anti-proton
c) Energy loss of anti-proton by collision
d) Differential cross section in cm

the atomic unit, $e = 1, \hbar = 1, m_e = 1$

*Refs on atomic structural effects. Refs on applications to molecules and crystals are not shown.

Details: $\frac{d\sigma}{d\Omega_{cm}} = \frac{4}{(q^2+\lambda^2)^2} \rightarrow -\frac{dW(E_{\bar{p}})}{dt} = \frac{4}{3\pi}(\epsilon V)^2 \cdot \ell og\sqrt{p_F} \cdot \xi(p_F)$,

with $\lambda = 4p_F/\pi$

$\xi(p_F) = \frac{\ell og(\pi p_F + 1) - \pi p_F/(\pi p_F + 1)}{2\ell og\sqrt{p_F}} \rightarrow 1$ for $p_F \gg 1$

Fermi Teller model

Radiation energy loss is thus contributed mostly from Keplerian orbits of small ℓ in the capture.

$$-\frac{dW^R}{dt} = \frac{2}{3}\frac{(\ddot{\varepsilon r})^2}{c^3} \rightarrow -\delta W^R = \frac{2\pi e^2 Z^4 \mu}{c^3 l^5}\left(1 + \frac{2El^2}{3\mu Z^2}\right)$$ per swing

together with $-\frac{dl}{dt} = -\frac{dW}{dt} l/MV^2$

$\delta E/E = 2\delta\ell/\ell$ from a basic kinematic argument.

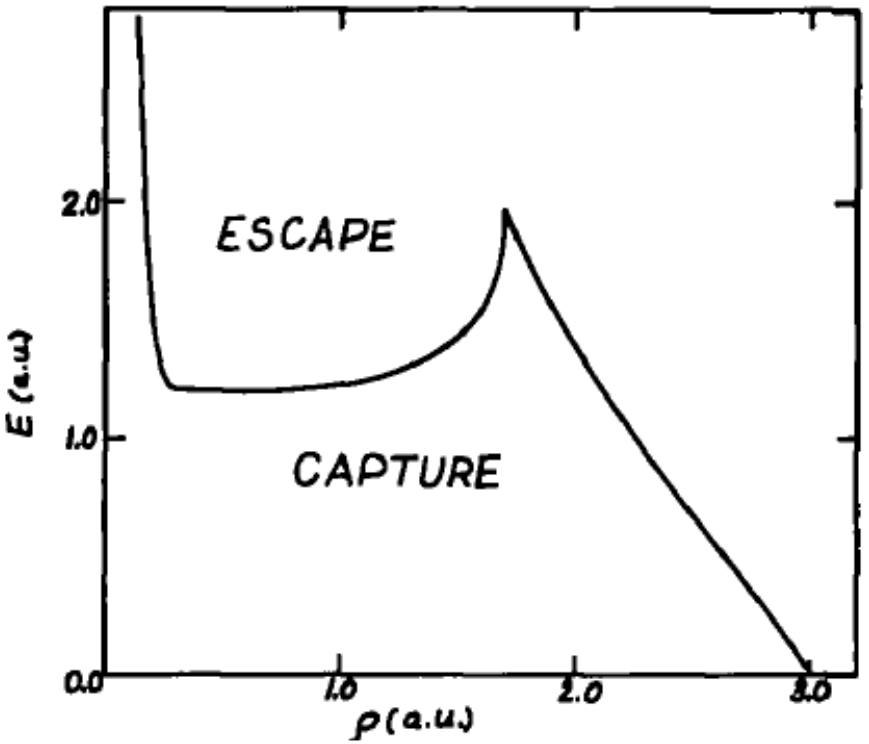

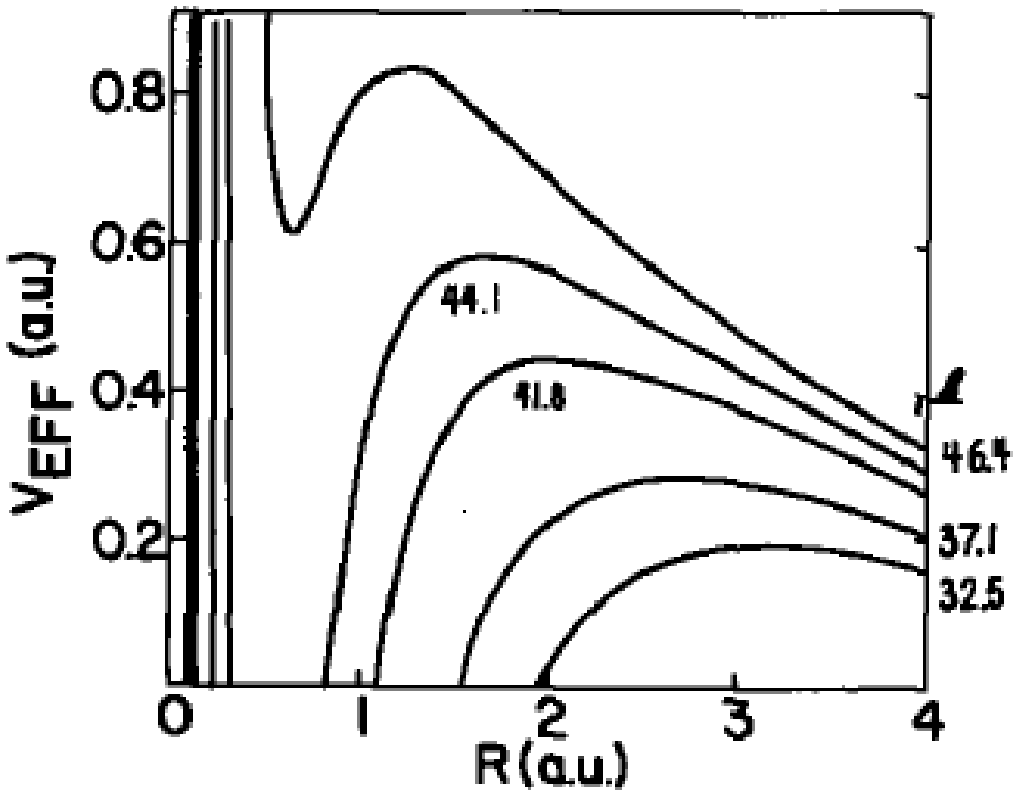

Fig. 3. Effective radial potential for different l.

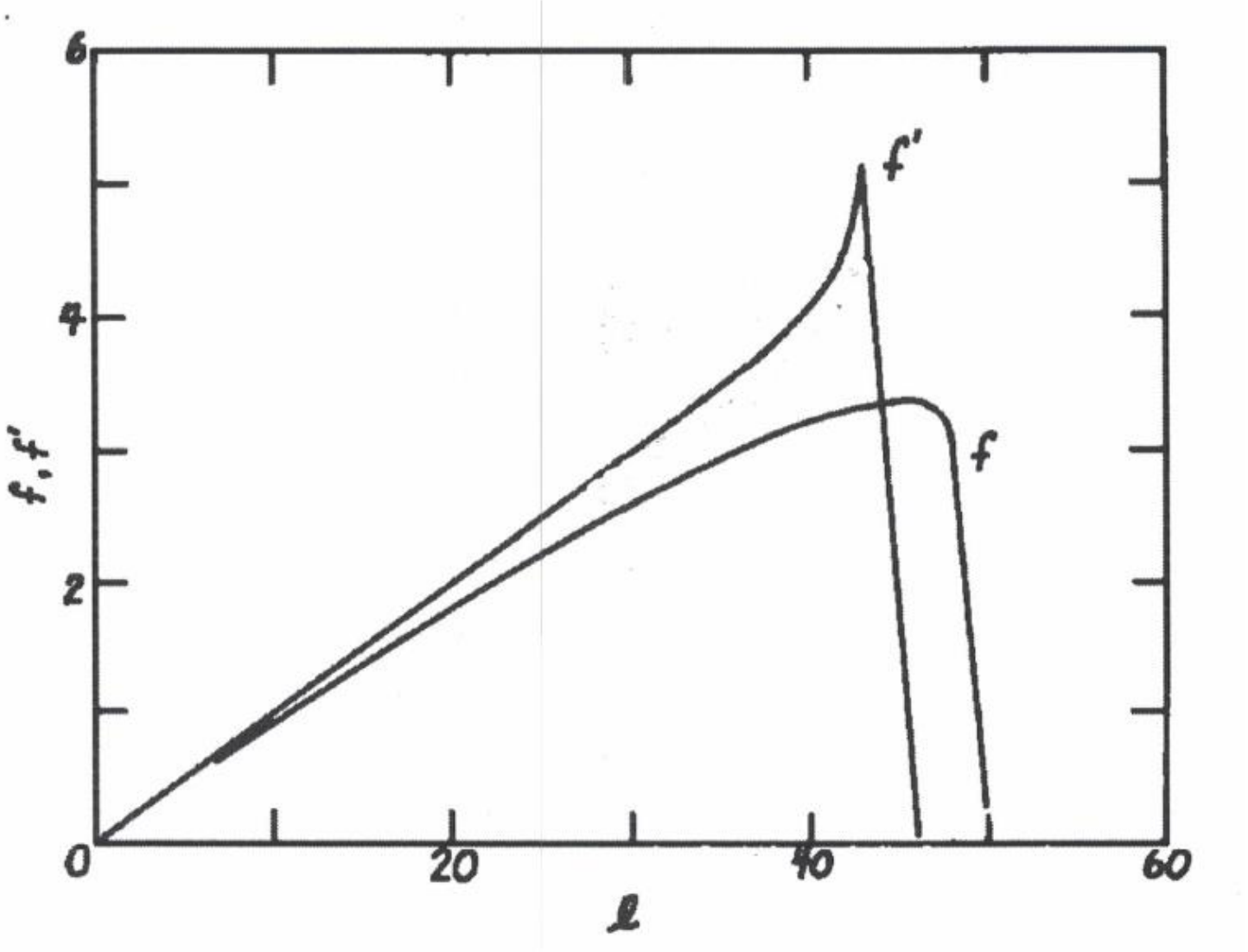

Integration over
the incident energy E_p and
the impact parameter ρ
yields

Capture f
for $E_p > 0$

Starting cascade f'
at $E_p = 0$

Atomic cascade

E and ℓ distribution (probability) function F(E, η) [η ≡ ℓ / ℓ(max)]
thus calculated obeys the equation of continuity (conservation of probability)

$$\frac{\partial F}{\partial E} + \frac{\partial}{\partial \eta}\left(F \frac{\mathrm{d}\eta}{\mathrm{d}E}\right) = 0.$$

for lowering E and ℓ

normalized for each E (<0): $\int_0^1 F(E, \eta)\mathrm{d}\eta = 1.$

⟶ with some variation, F(E, η) is found to be similar to
the 2ℓ+1 distribution, as going through the electron cloud

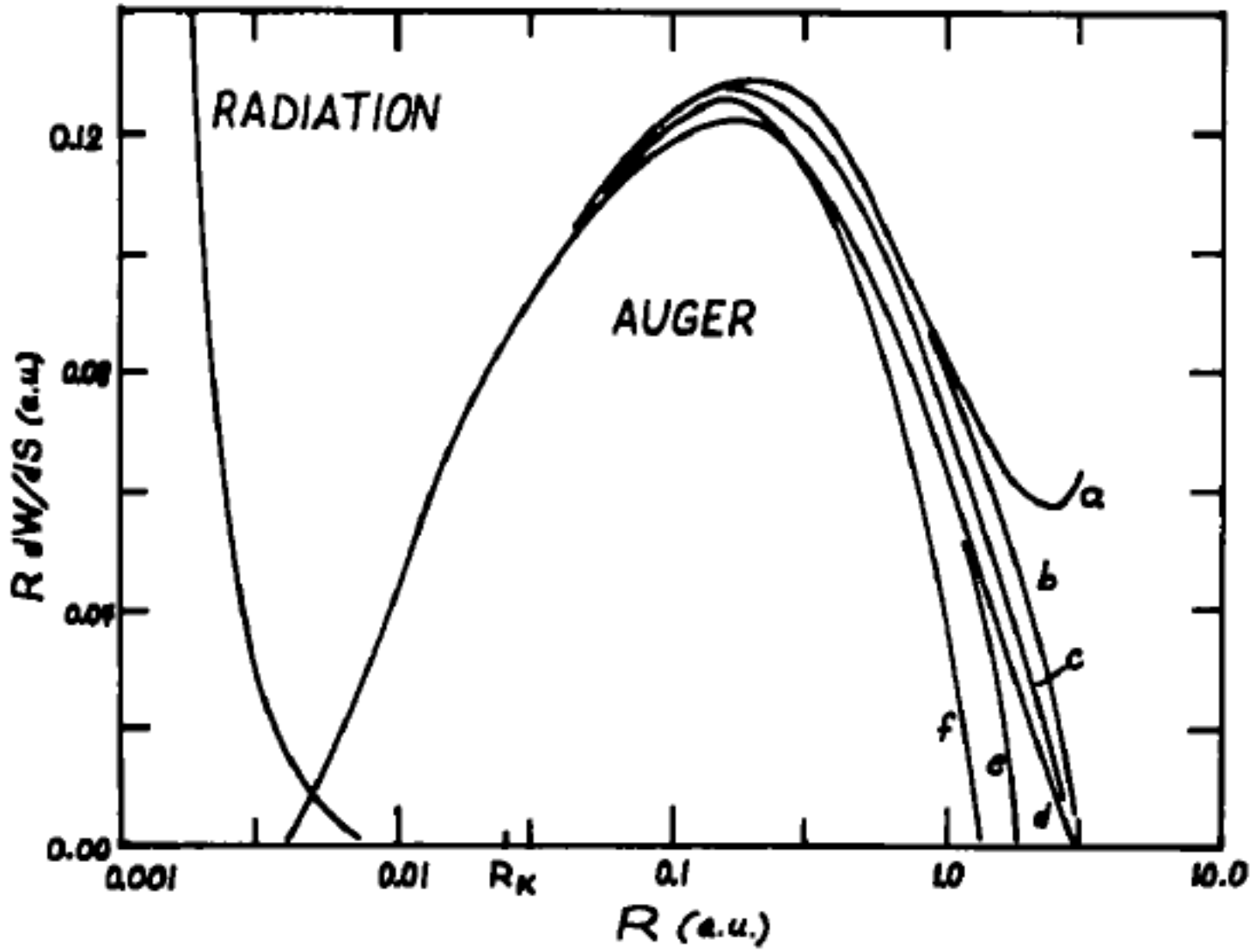

R(a.u) =1
= 0.53 Å

Fig. 1. Radiative and Auger energy loss. Curve (a) corresponds to eq. (6′) with $\varepsilon_s = 0.5$, (b) to eq. (6′) with $\varepsilon_s = 0.0$, (c) to eq. (9′) with $\varepsilon_s = 0.0$, (d) to eq. (8′) with $\varepsilon_s = 0.5$, (e) to eq. (8′) with $\varepsilon_s = 0.0$, and (f) to the generalization of eq. (6′) that includes the effect of an energy gap of 0.3 with $\varepsilon_s = 0.0$.

F at K-shell

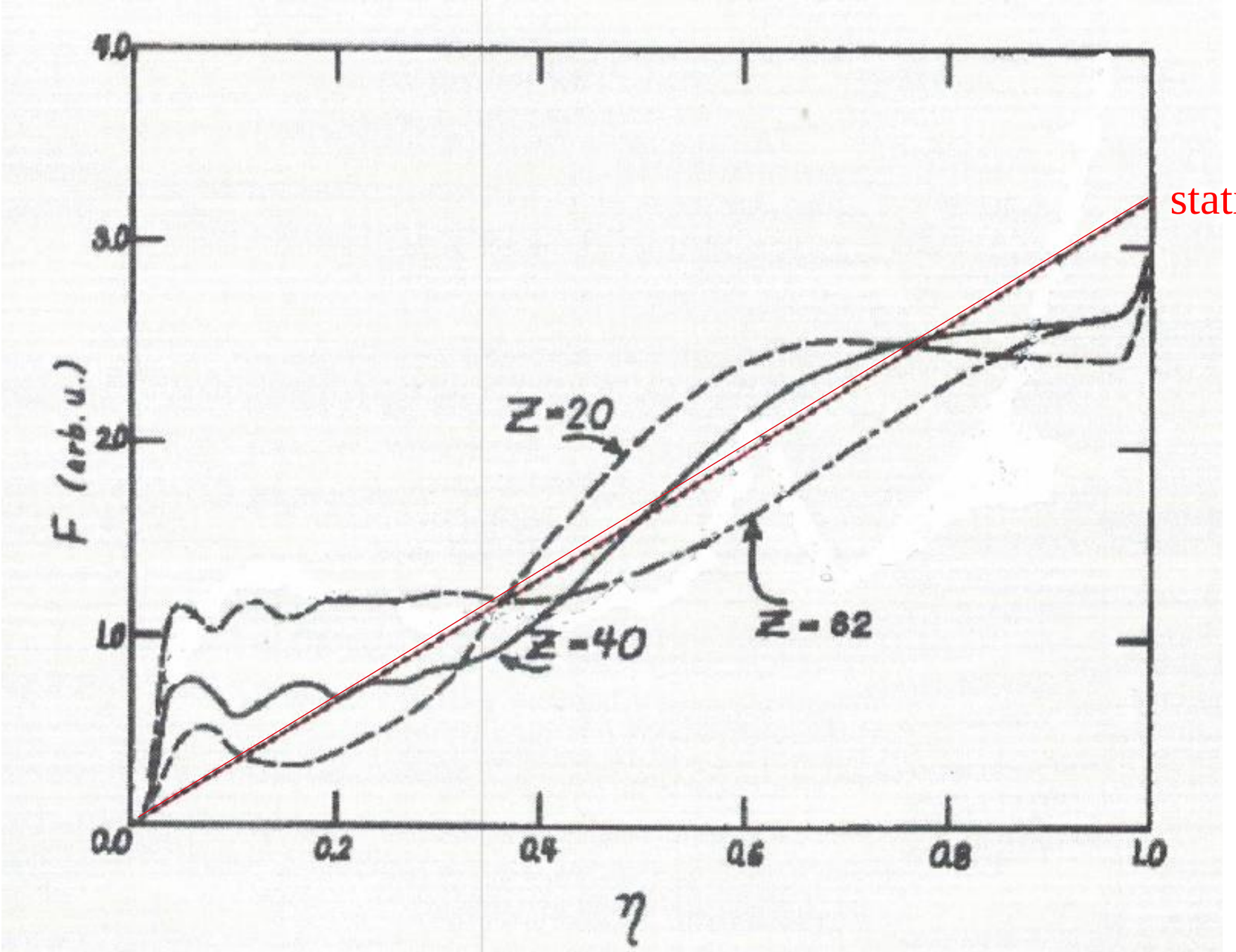

statistical

Subsequent works on Fermi-Teller model

- M. Leon, J. Miller, *Nucl. Phys*. **A282**, 461 (1977).
- H. Daniel, *Ann. Phys*. **129**, 303 (1980)

Leon-Miller

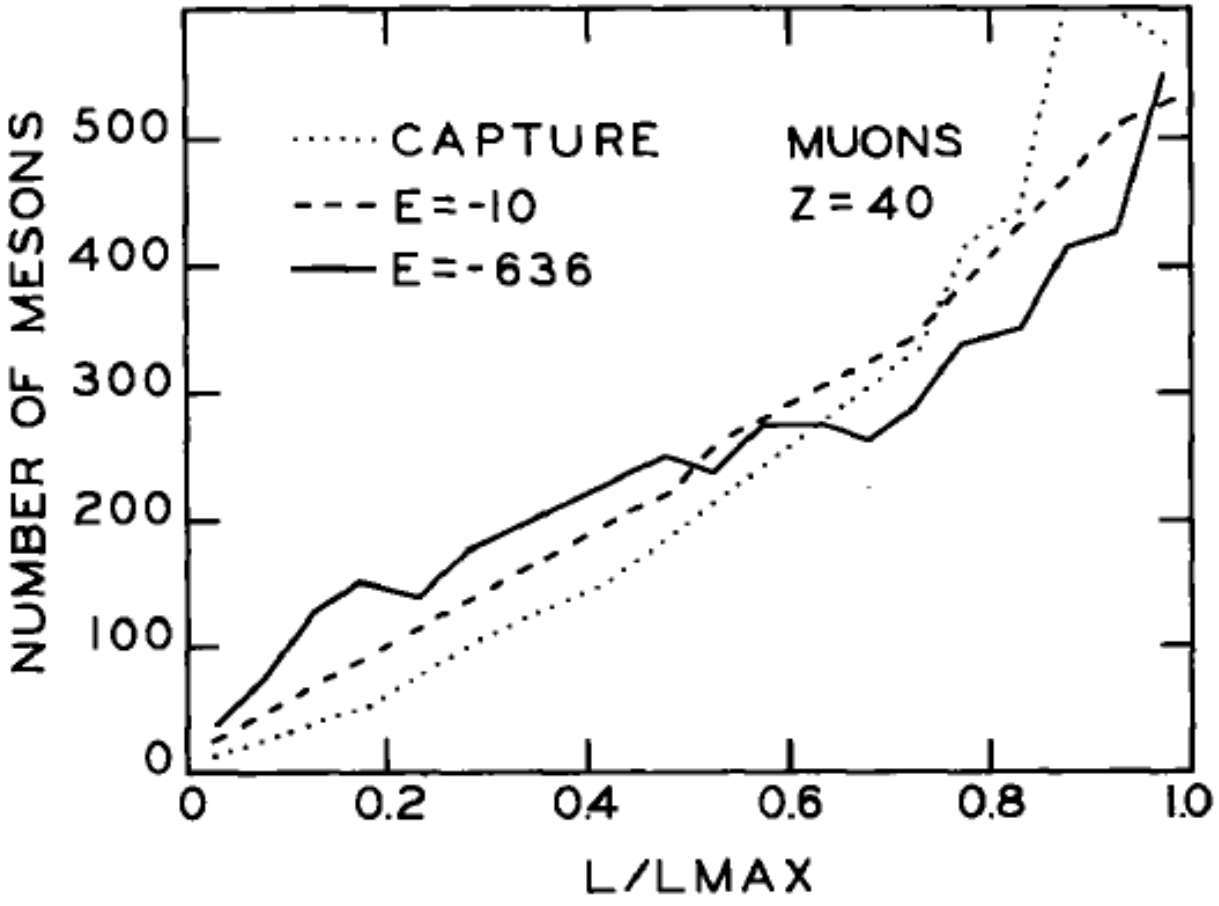

Change in the angular momentum distribution after capture.

Other than Fermi-Teller model

FMD (fermion molecular dynamics)

using Kirschbaum-Wilets model* of atoms.

J. Cohen, *Phys. Rev.* **A65**, 052714 (2002).

* C. Kirschbaum, L. Wilets, *Phys.Rev.* **A21**, 834 (1980).

On atomic capture but no cascade.

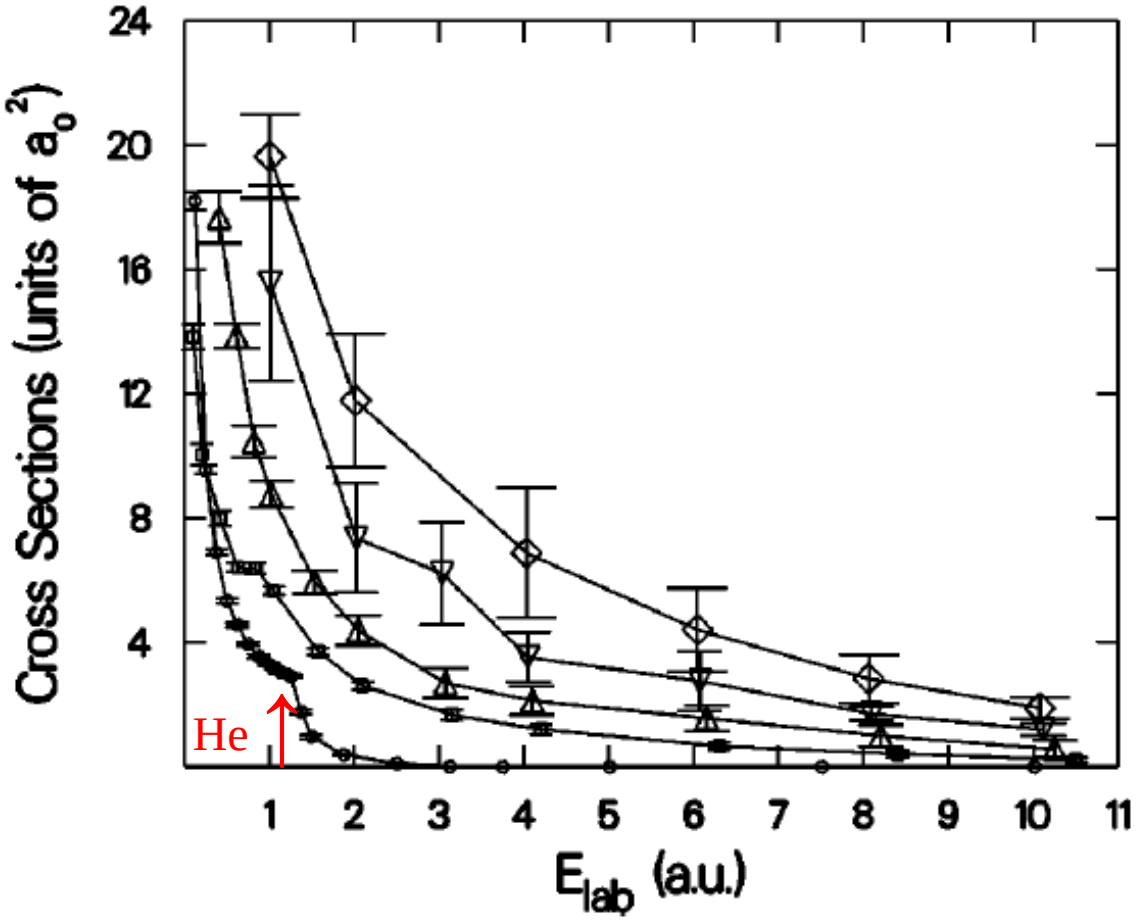

FIG. 2. Cross sections for antiproton capture by He (circle), Ne (square), Ar (up triangle), Kr (down triangle), and Xe (diamond) as a function of incident antiproton energy, with Monte Carlo error bars of the FMD calculation.

3. Atomic Capture

Extensive calculations of **light anti-protonic atoms,** H and He,*

Adiabatic potential + centrifugal potential between anti-proton and Z^+

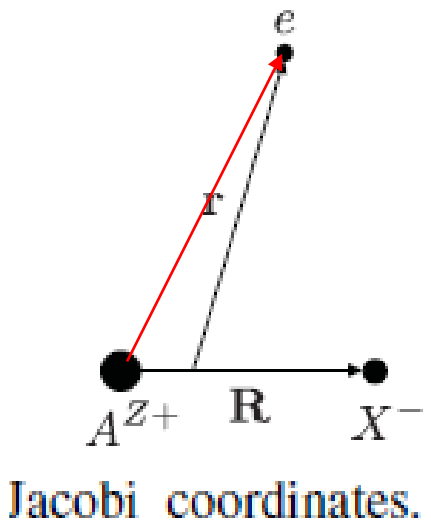

Jacobi coordinates.

K.Sakimoto, *Phys.Rev.* **A**82, 012501 (2010)

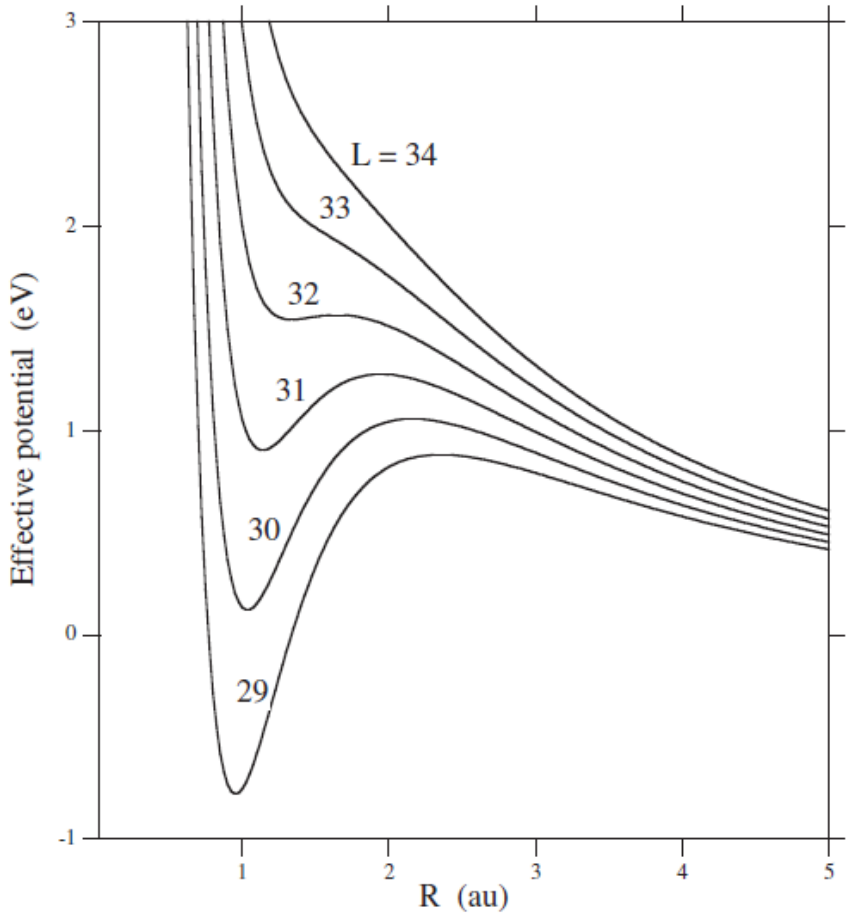

K.Sakimoto, *J. Phys.* **B** 34, 1769 (2001)

Capture probability seems dominant

around E_p = the barrier height of effective potential

* Review and refs. prior to 2004, see J. Cohen, Rep. Prog. Phys. 67, 1769 (2004).

Recent progress: H and He atomic capture by

QM 3-body calculation, using mostly adiabatic approximation (~Born-Oppenheimer approx.) in the initial state.

N. B. The final state is mostly two-body in a definite Q state.

H: **$p' + H \rightarrow p'p + e$** protonium formation; K. Sakimoto, *Phys. Rev.* **A88**, 012507 (2013) and refs quoted therein.

He: **$p' + He \rightarrow p'+He^{+} + e$** (R-matrix calculation) K. Sakimoto, *Phys. Rev.* **A91**, 042502 (2015)

$\rightarrow (p'He^{+}) + e$ Meta-stable state with precision laser spectroscopy for precision proton mass determination & PCT test.

Many refs. + the recent, M. Hori, *EPJ Web of Conf.* , 01001 (2018)

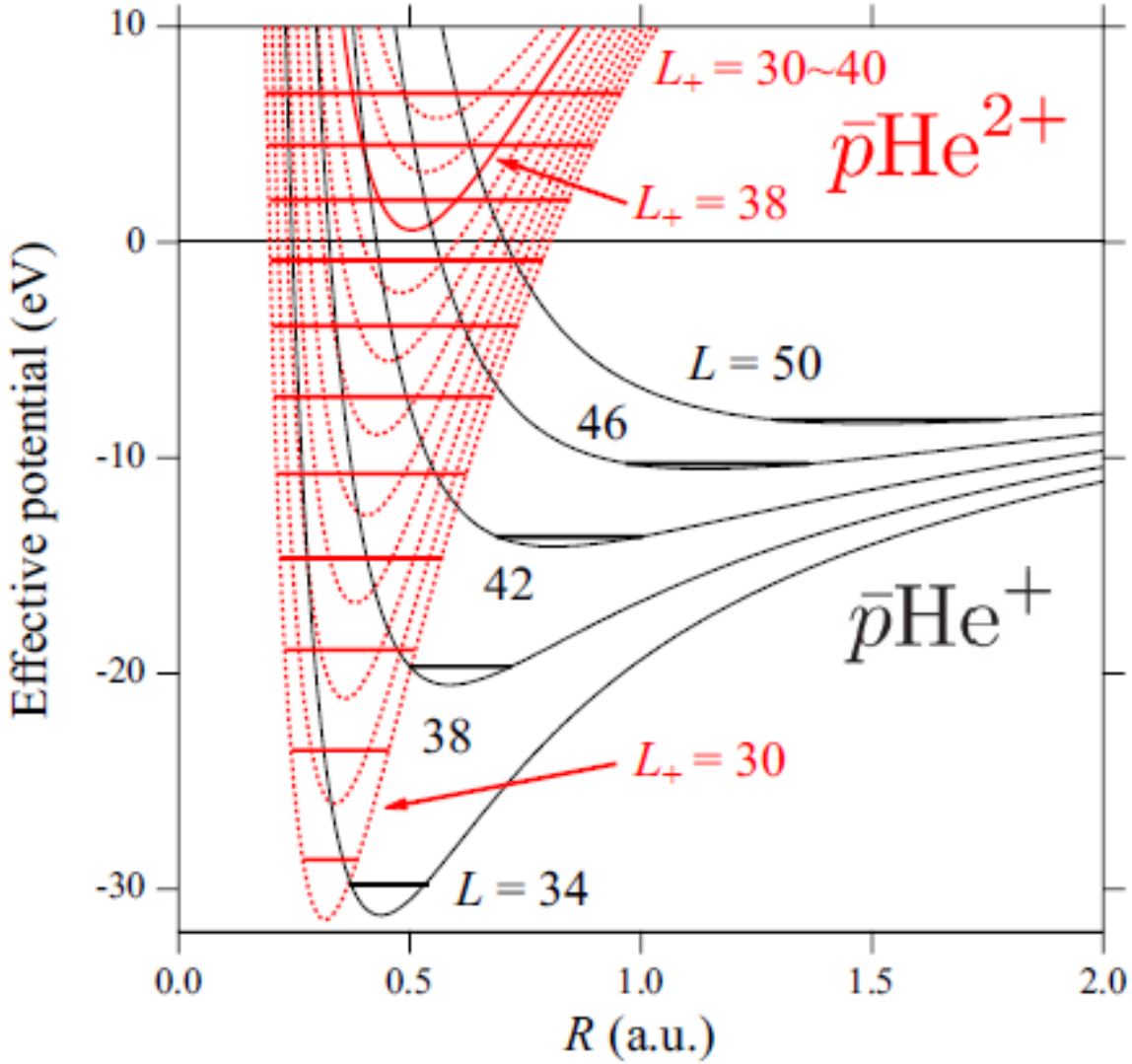

FIG. 3. (Color online) Effective potential energies of $\bar{p} + \mathrm{He}^+$ ($L = 34,38,\ldots,50$) and $\bar{p} + \mathrm{He}^{2+}$ ($L_+ = 30,31,\ldots,40$), measured from the dissociation limit ($\bar{p}\mathrm{He}^+ \rightarrow \bar{p} + \mathrm{He}^+$). Horizontal lines indicate several energy levels of $\bar{p}\mathrm{He}^+(N = L+1, L)$ (i.e., $v = 0$) and $\bar{p}\mathrm{He}^{2+}(N_+, L_+)$.

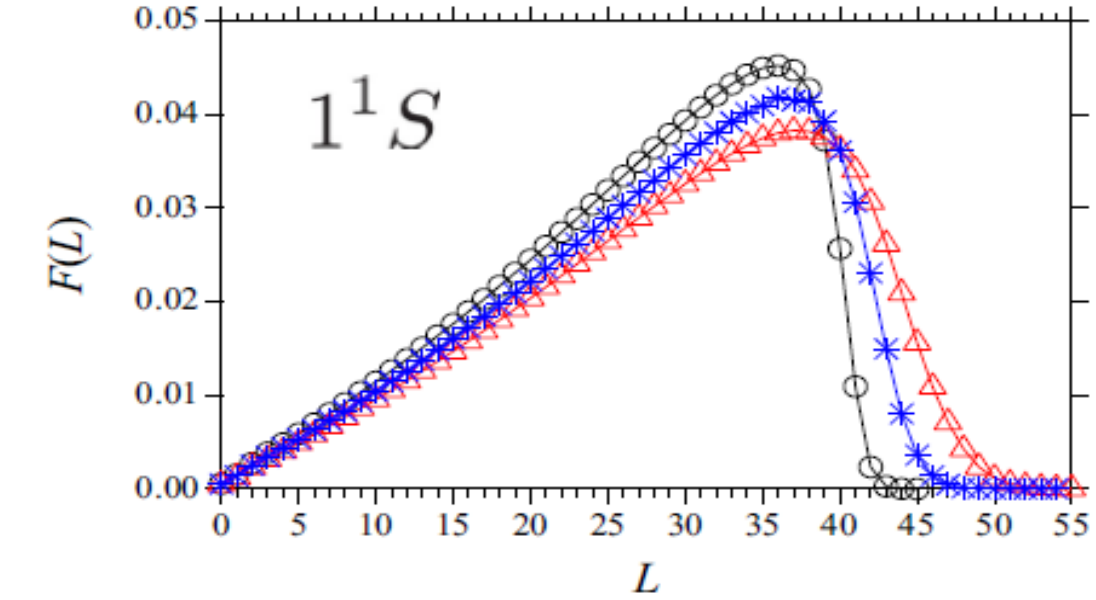

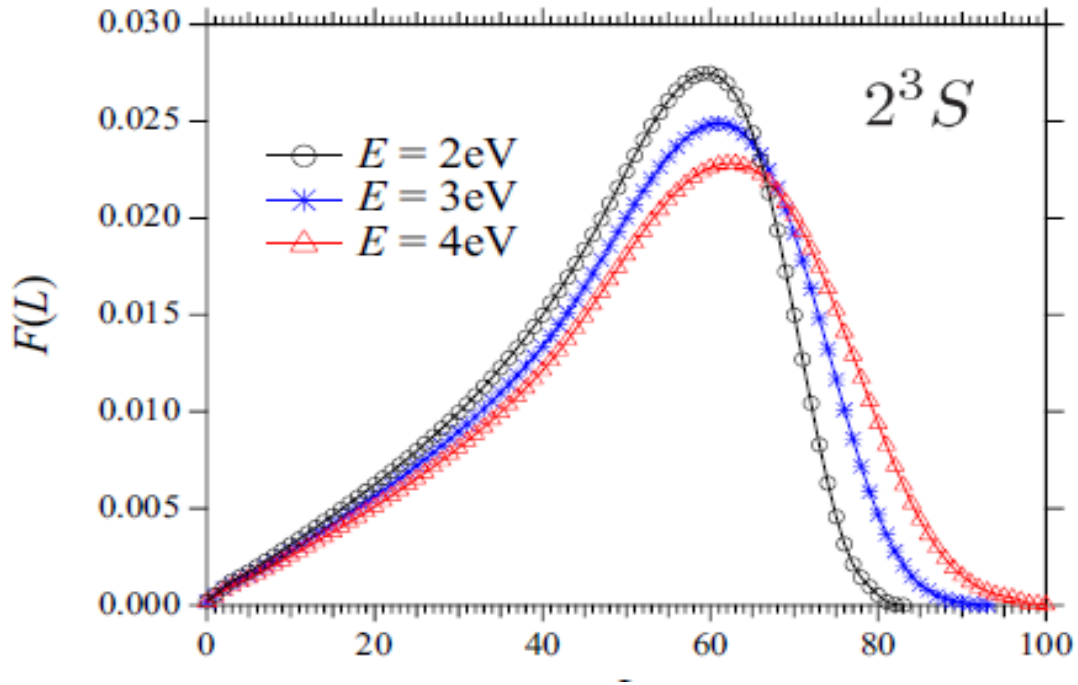

Some previous **light atoms** calculations on the ℓ dependence of capture probability,.
most showing approximate proportionality to 2ℓ +1

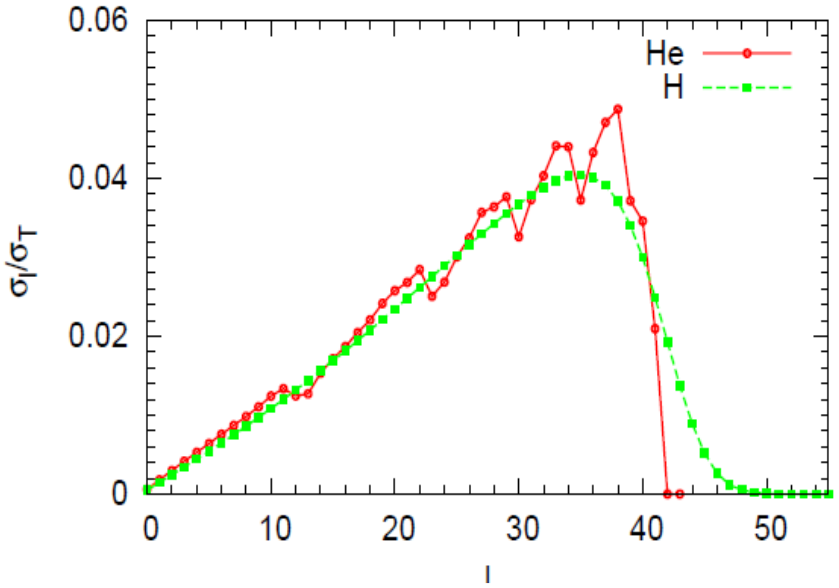

pbar – H, He capture cross section
Tong, Hino,Toshima (2009)

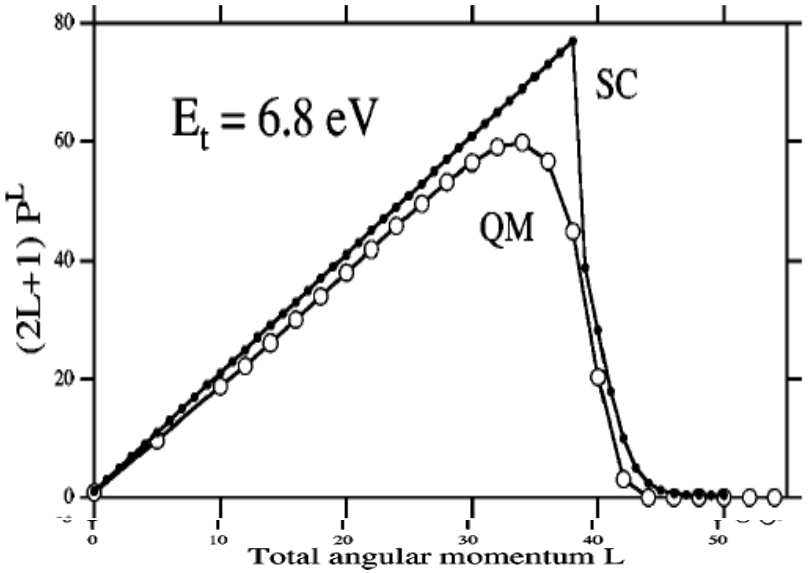

pbar – H opacities
Sakimoto (2001)
QM

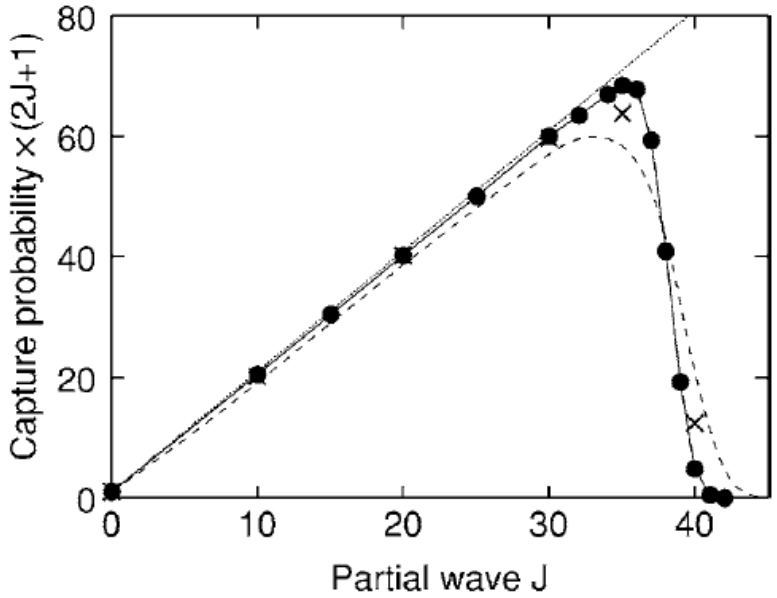

pbar– H capture probability
Yamanaka,Ichimura (2006)
Three-body QM by CCA

Channel-coupling-array

Seemingly, nature wants 2ℓ +1 in capture.

Comparison of nuclear and atomic processes as three-body reactions

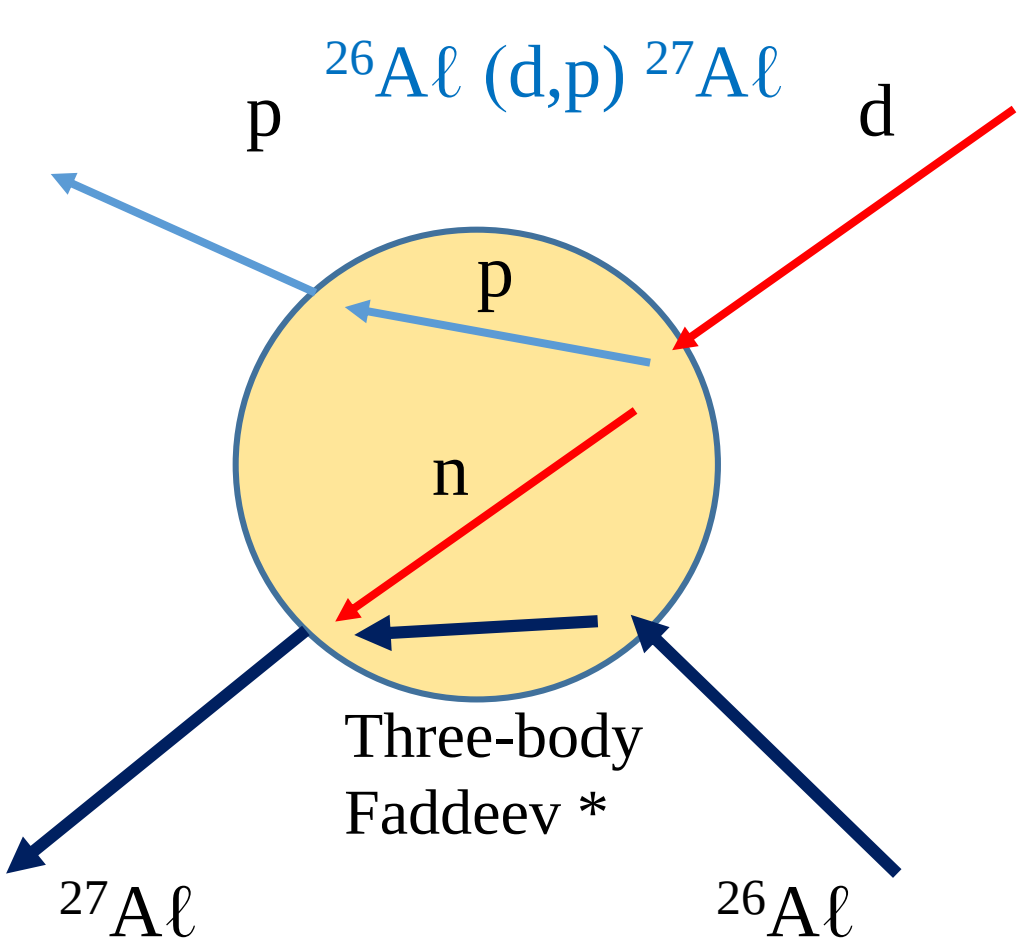

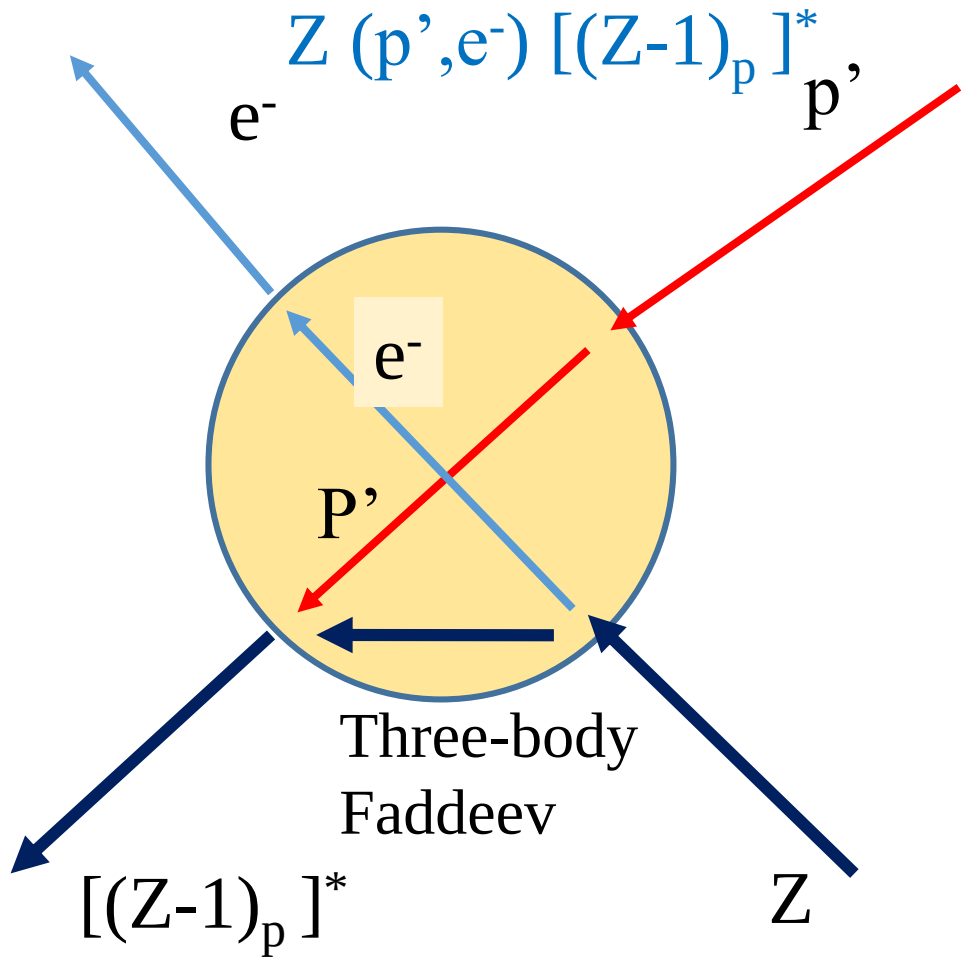

*A. Deltuva, *Phys. Rev*. **C79**, 021602(2009); ibid., **C98**, 021603(2018). [Adiabatic DWA}
M. Gomez-Ramos, N. Timofeyuk, *Phys. Rev.* **C98**, 011601®(2018)&arXiv;1905.13451(2019) [CDCC]

Continuum-discretized
Coupled channel

3. Atomic cascade

a) Atomic structure is NOT that of Bohr atom of

Z^+ nucleus + Z-1$^-$ electrons + an anti-proton.

$$M_{\bar{p}} = 938.272 \text{ MeV}$$

$$m_e = 0.510999 \text{ MeV}$$

$$\rightarrow \quad \xi \equiv \sqrt{\frac{M_{\bar{p}}}{m_e}} \approx 42.85$$

$$B.E. = \frac{(Ze^2)^2 m}{2\hbar^2 n^2}$$

$$R = \frac{n^2\hbar^2}{Ze^2 m}$$

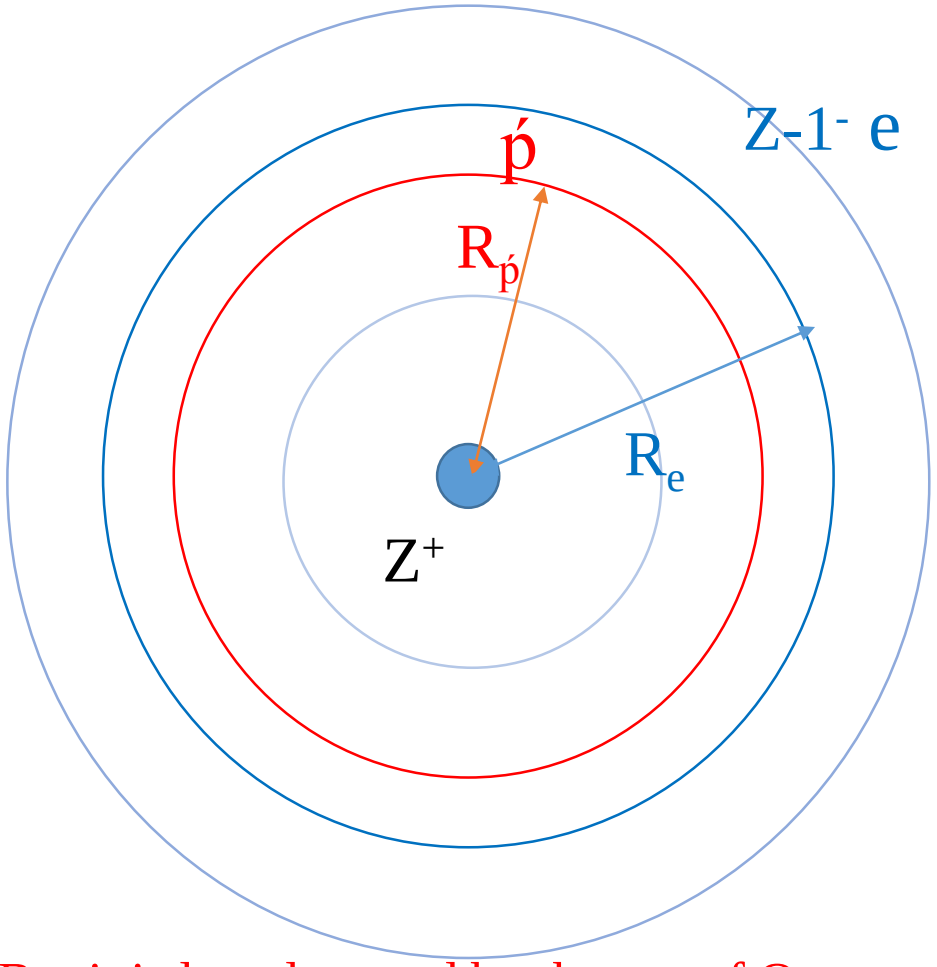

$$\frac{n_{\bar{p}}}{n_e} = \xi$$

$$\frac{R_{\bar{p}}}{R_e} = 1$$

e and $\bar{p}$ of the same R

$\rightarrow$ the same $B.E$

with different $n's$ of ξ

Unrealistic!

But it is largely cured by the use of Q.-state dependent effective charges Z*.

b) A simple view:

Compare

- the energy loss of the anti-proton during the cascade (computation) and
- the ionization energies by possible Auger process

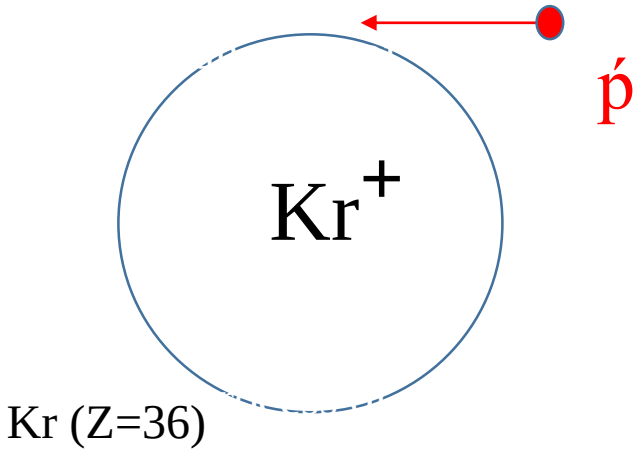

capture

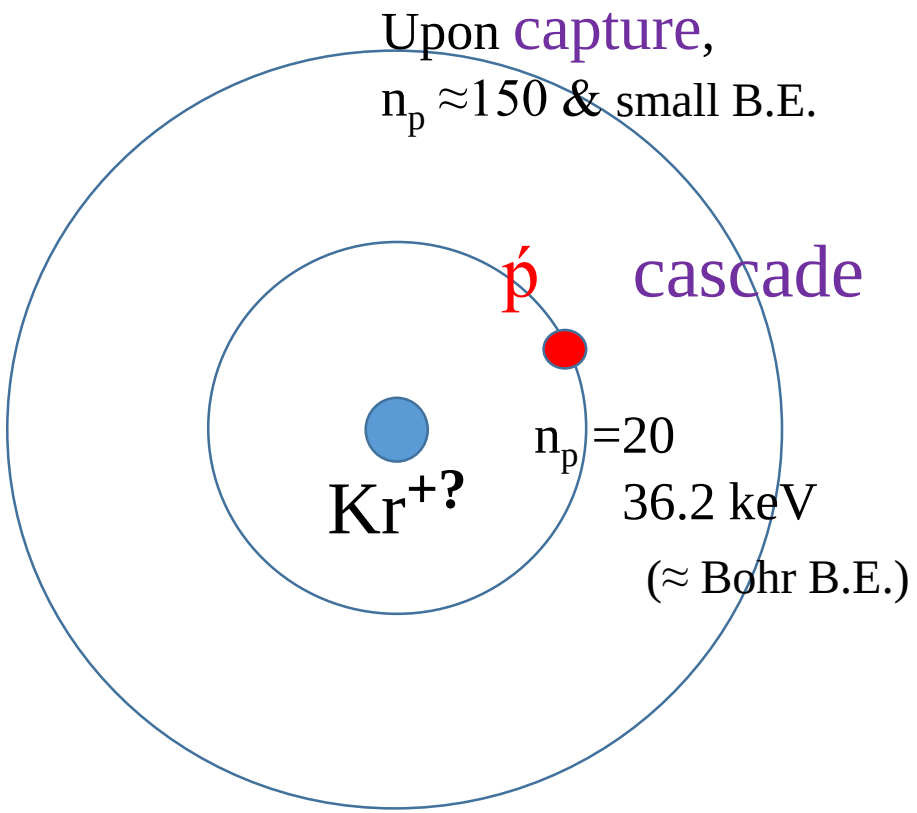

Between capture and $n_p \approx 20$ (the start of cascade computation),
the energy difference ≤ 36 keV

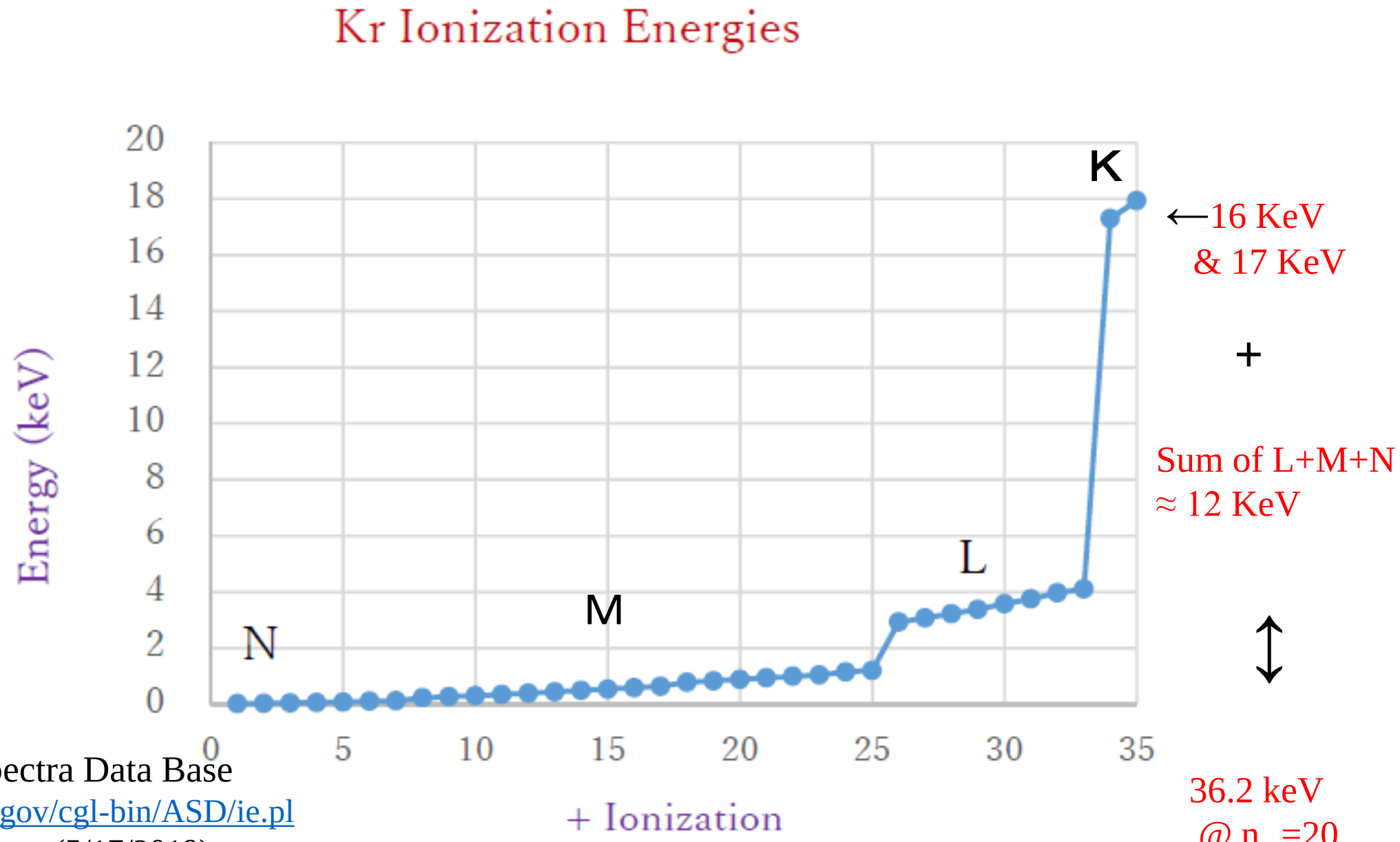

NIST Atomic Spectra Data Base
http://physics.nist.gov/cgl-bin/ASD/ie.pl
(5/17/2019)

2) Prominent K-edge effects

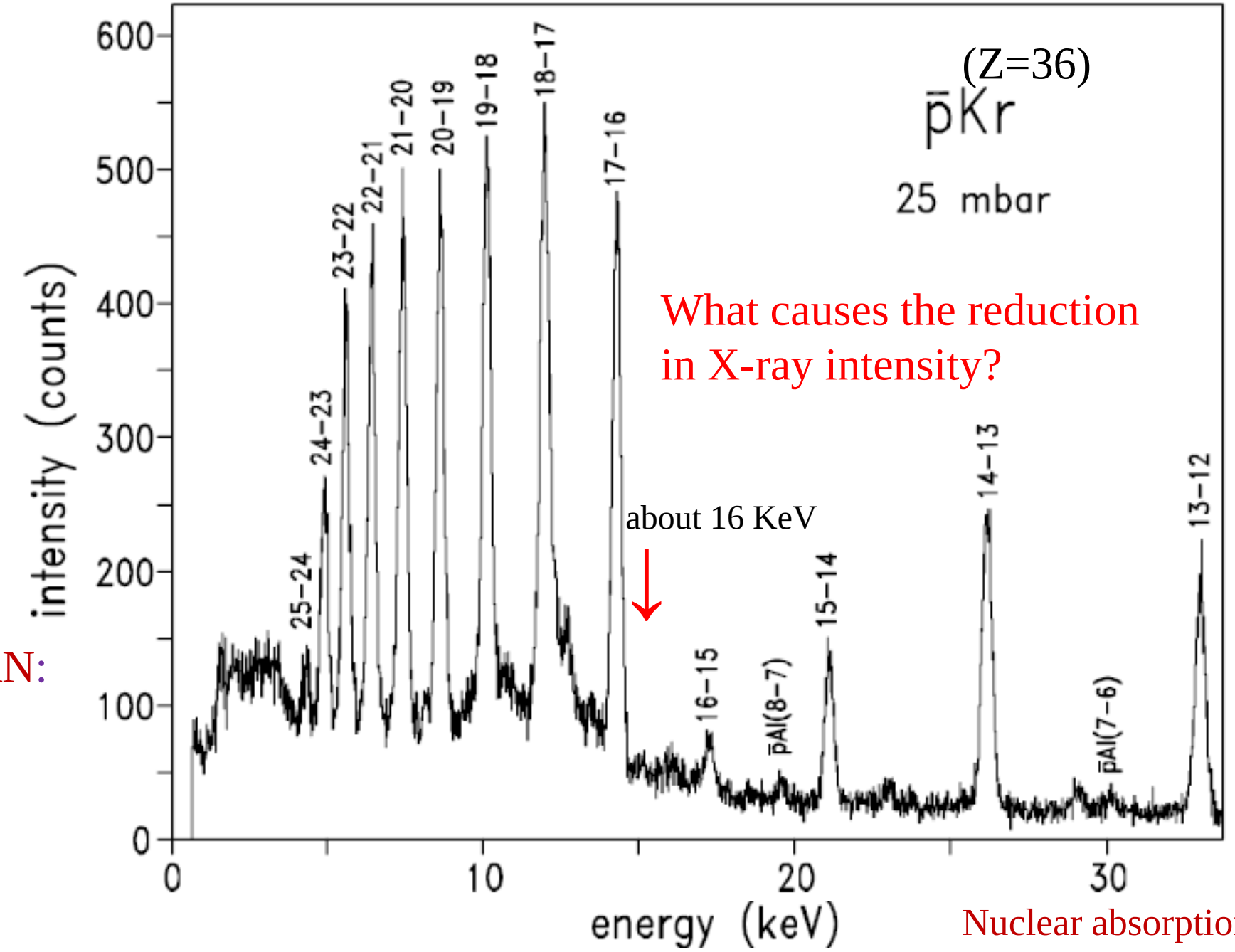

LEAR PS175 at CERN:
D. Gotta et al.
Eur. Phys. J.,
D47, 11 (2008);
and refs.therein.

Nuclear absorption →

The reduction is not because of nuclear absorption:

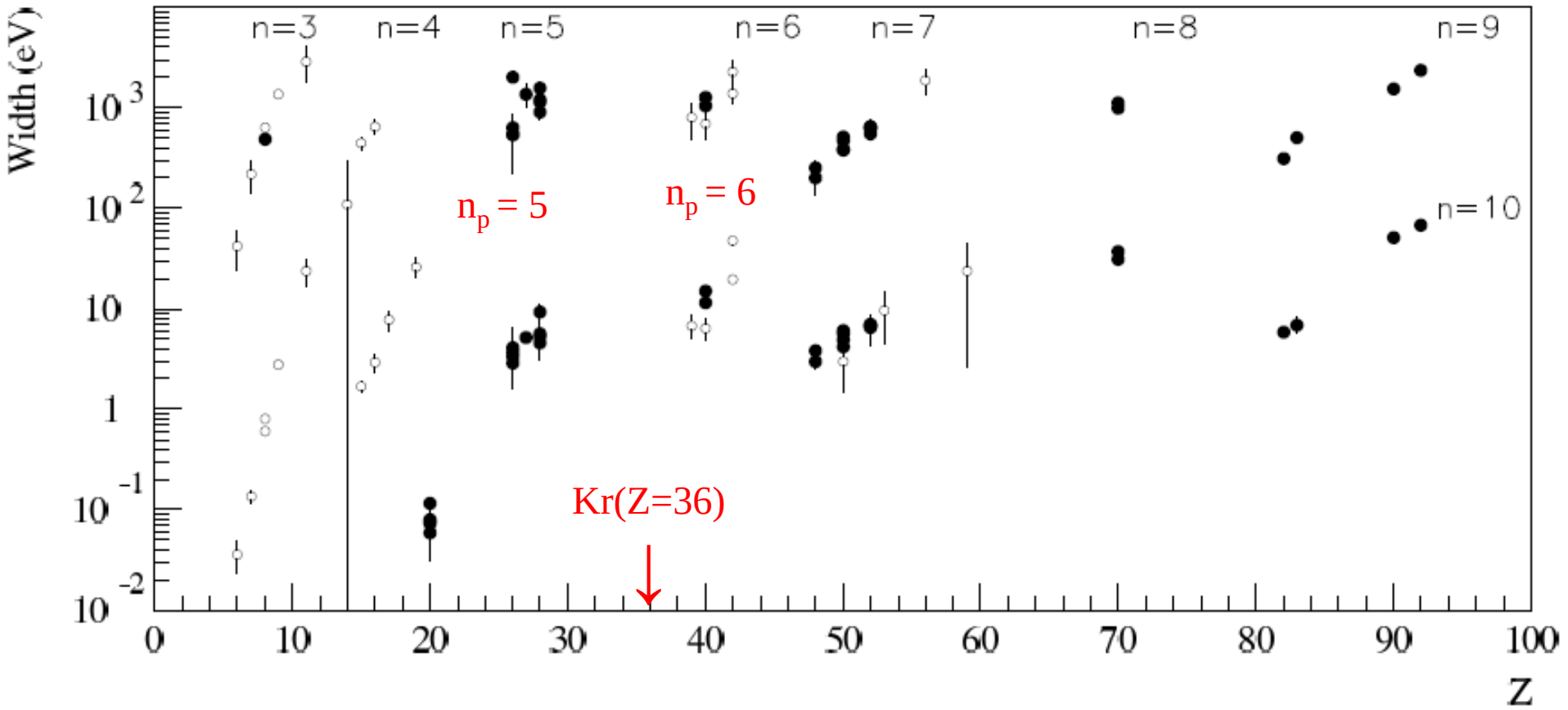

Fig. 1. Antiprotonic strong interaction level widths as a function of atomic number Z. Full circles — values determined in the PS209 experiment; open circles — earlier data [9].

A. Trzcinska for the PS209 Collaboration, *Acta phys. Polonica* **B41**, 311 (2010)

The reduction is not
because of detector efficiency.

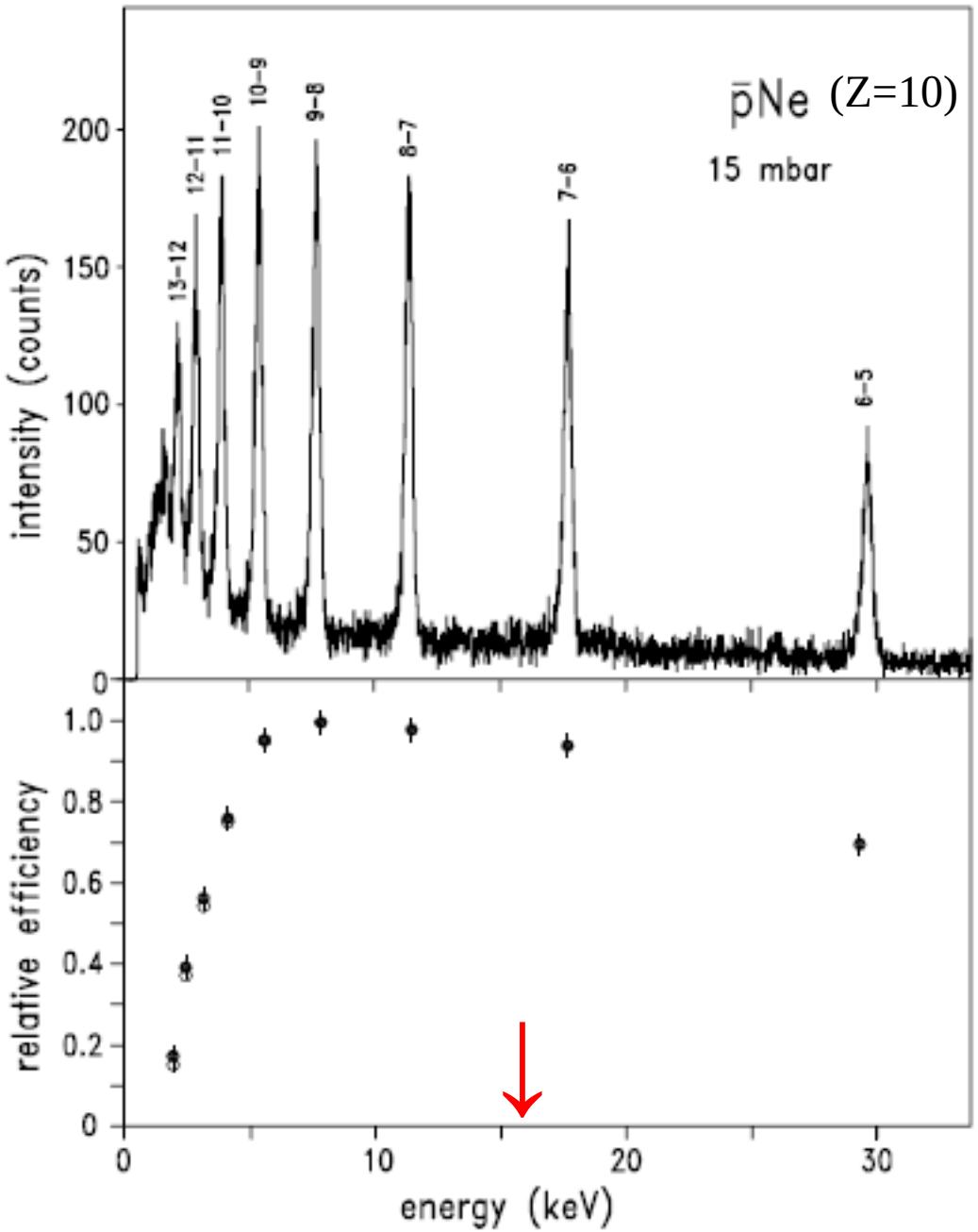

D. Gotta et al. (2008) *ibid.*

Ferrell's formula*:

Relation in dipole approx. between

Γ_A Auger emission rate and

Γ_X radiative (X-ray) transmission rate:

$$\Gamma_A/\Gamma_X = \sigma_{\gamma e}^{(Z^e_{eff}-1)}(E)/[(Z^e_{eff}-1)^2\sigma_T]$$

$\sigma_{\gamma e}(E)$ photoelectric cross section

σ_T Thomson cross section

Z^e_{eff} effective charge seen by the electron

*R. Ferrell Phys. Rev. Lett. 4, 425 (1960).

Z and X-ray energies (eV) for $\Gamma_A / \Gamma_X = 0.5, 1, \& 2$

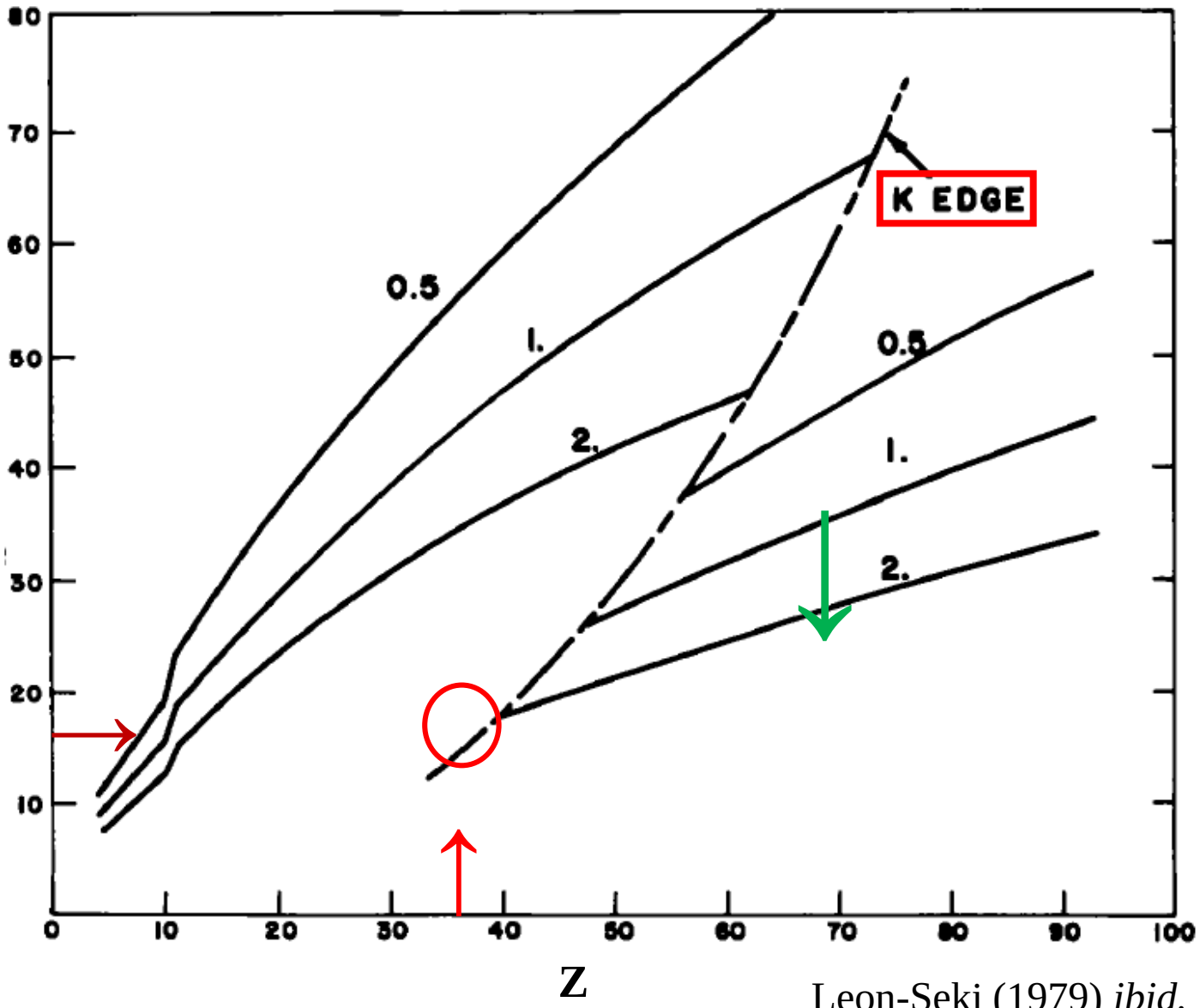

Leon-Seki (1979) *ibid.*

$$\Gamma_X \propto \Delta E^3$$

$$\Gamma_A \propto 1/\sqrt{E}$$

"equivalent photon flux" given by *

$$I = \frac{c}{2\pi\hbar\omega}\left(\frac{m}{e}\right)^2 \omega^4 (Z-1)^{-2} \sum_f |\vec{\mathbf{r}}_{fi}|^2$$

$$= (Z-1)^{-2}\, \sigma_T^{-1}\, w_R,$$

$$\rightarrow \quad w_A/w_R = (Z-1)^{-2}\, \sigma_{Z-1}/\sigma_T.$$

*R. Ferrell (1960) *ibid.*.

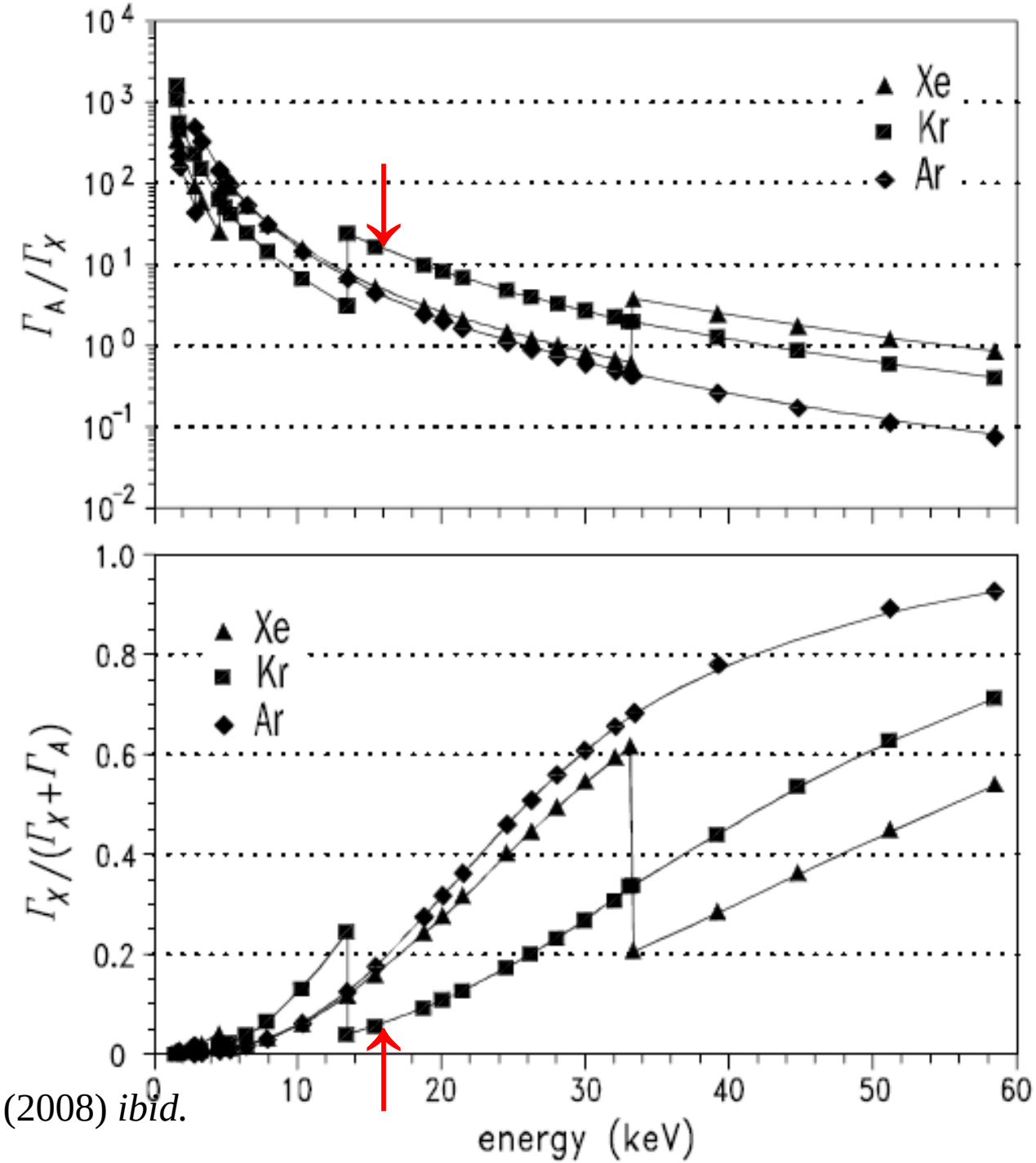

D. Gotta et al. (2008) *ibid.*

Direct observation of Auger electrons: Difficult.

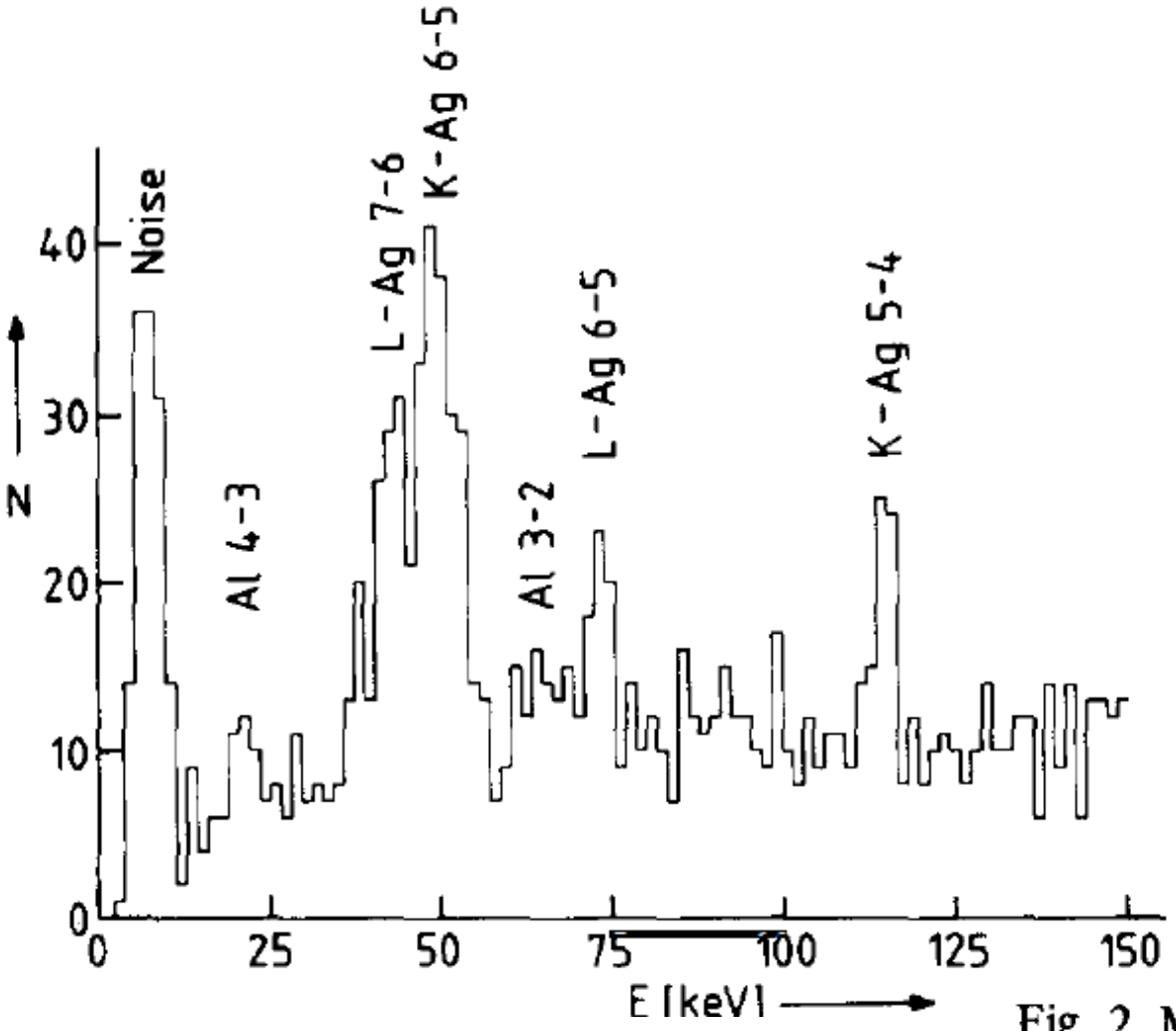

R. Callies et al., *Phys. Lett.* **A91,** 441 (1982)

Fig. 2. Muonic Auger spectrum from Ag. Number of counts versus energy E, one channel corresponding to 1.53 keV. The Al lines are X-ray lines.

Determination of realistic low-energy X-ray spectral lines of anti-protonic atoms in D. Gotta et al. (2008) *ibid.*

- Use of MCDF(multiconfiguration Dirac-Fock) approximation code* by P. Indelicato and J. Desclaux http://dirac.spectro.jussieu.fr/mcdf/mcdf_welcome/mcdf_homepage.html

[*Solving relativistic many-body problems in the Hamiltonian formulation including QED and finite-size nucleus corrections]

- Transitions of antiproton are included as a heavy classical particle in circular orbits of the radius R_p with the effective charge Z^P_{eff} at R_p in the MCDF atom:

Anti-proton has the effective charge in Kr;

$$Z^{\bar{p}Kr}_{eff}(R_{\bar{p}}) = 36.167e^{-0.579R_{\bar{p}}}$$

in the state of the principal quantum number

$$n_{\bar{p}} = \sqrt{R_{\bar{p}} Z^{\bar{p}}_{eff} m_{\bar{p}}/m_e}$$ in a.u

with the transition energy

$$\Delta E_{n_{\bar{p}} \to n_{\bar{p}}-1} = E_{Ryd} \frac{(Z^{\bar{p}}_{eff})^2 (2n_{\bar{p}} - 1)}{[n_{\bar{p}}(n_{\bar{p}} - 1)]^2}$$

$$E_{Ryd} = m_{\bar{p}} c^2 \alpha^2 / 2 = 24982.2 \text{ eV}.$$

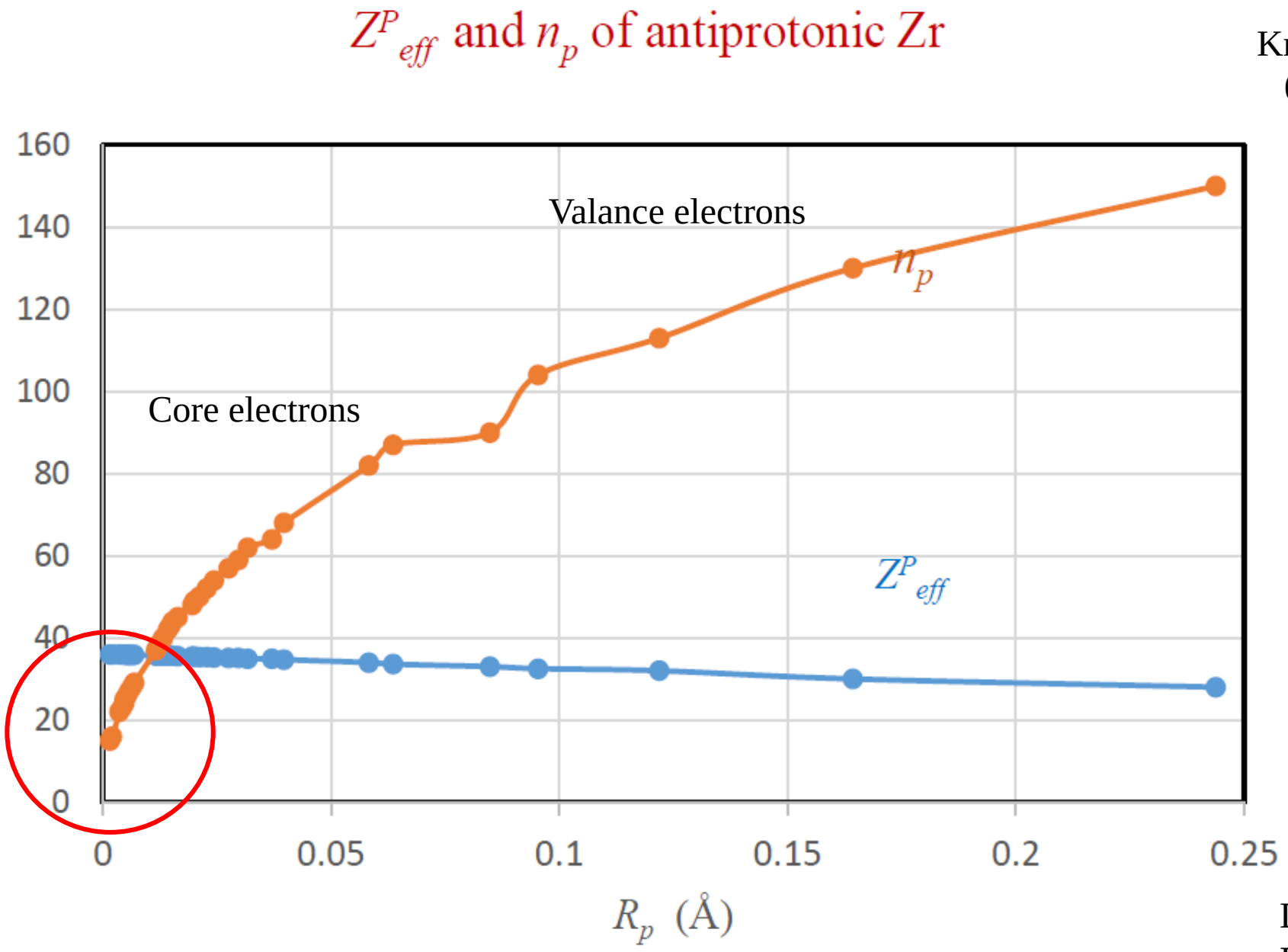

Kr Atomic radius
0.88 Å (Calculated)

N.B. In Bohr model,

$$R = \frac{n^2\hbar^2}{Ze^2m}$$

Drawn from Table 3
D. Gotta et al (2008) ibid

Transition and ionization energies

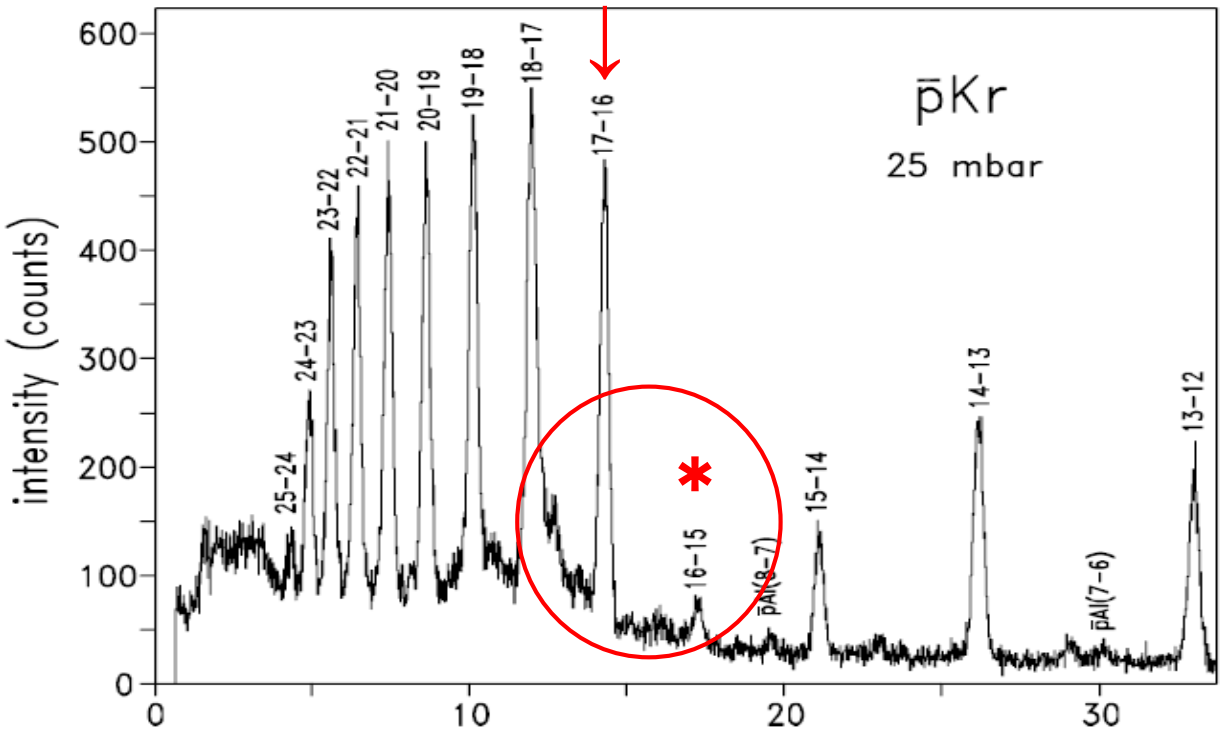

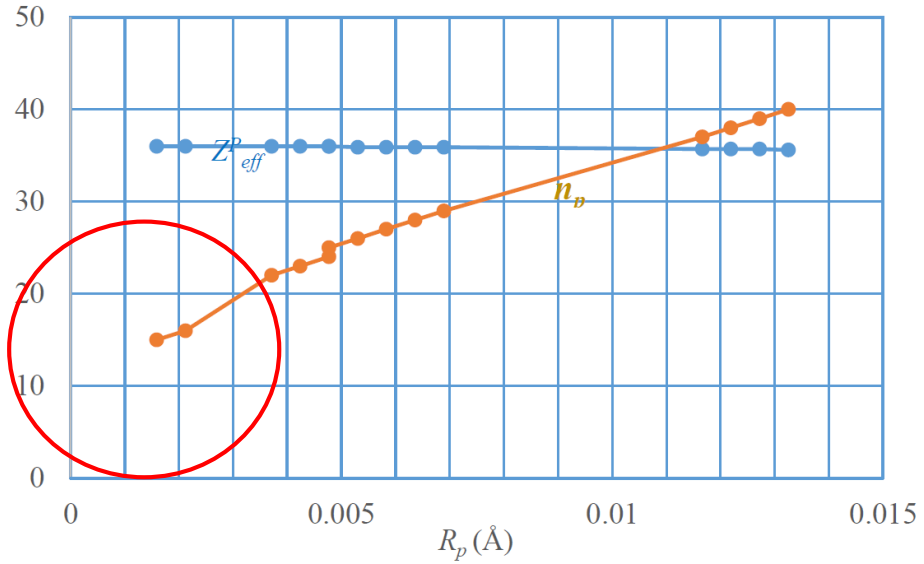

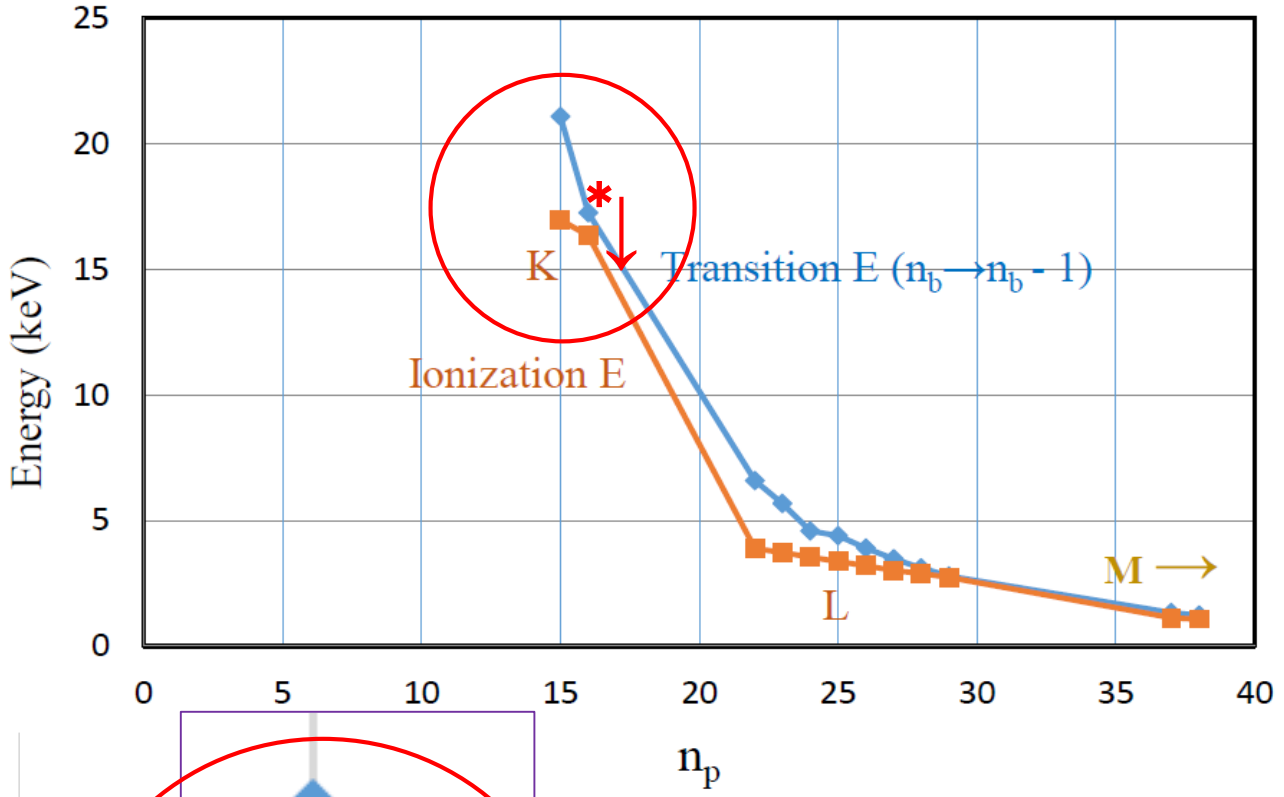

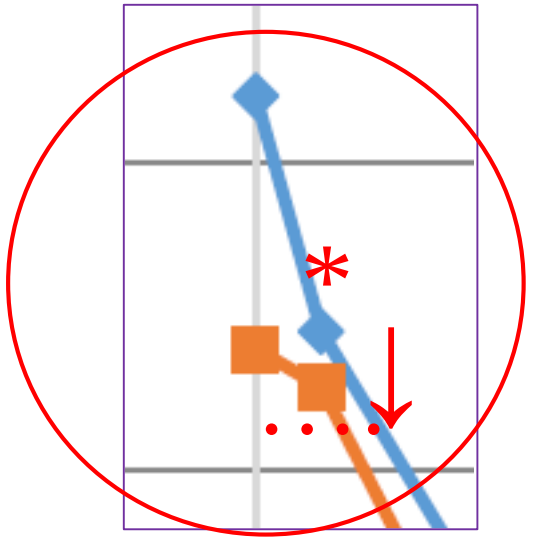

n_p =15 16 17

Appearance of K-edge effects

Drawn from Table 3
D. Gotta et al (2008) ibid

Appearance of K-edge effects in exotic-atom intensity spectroscopy

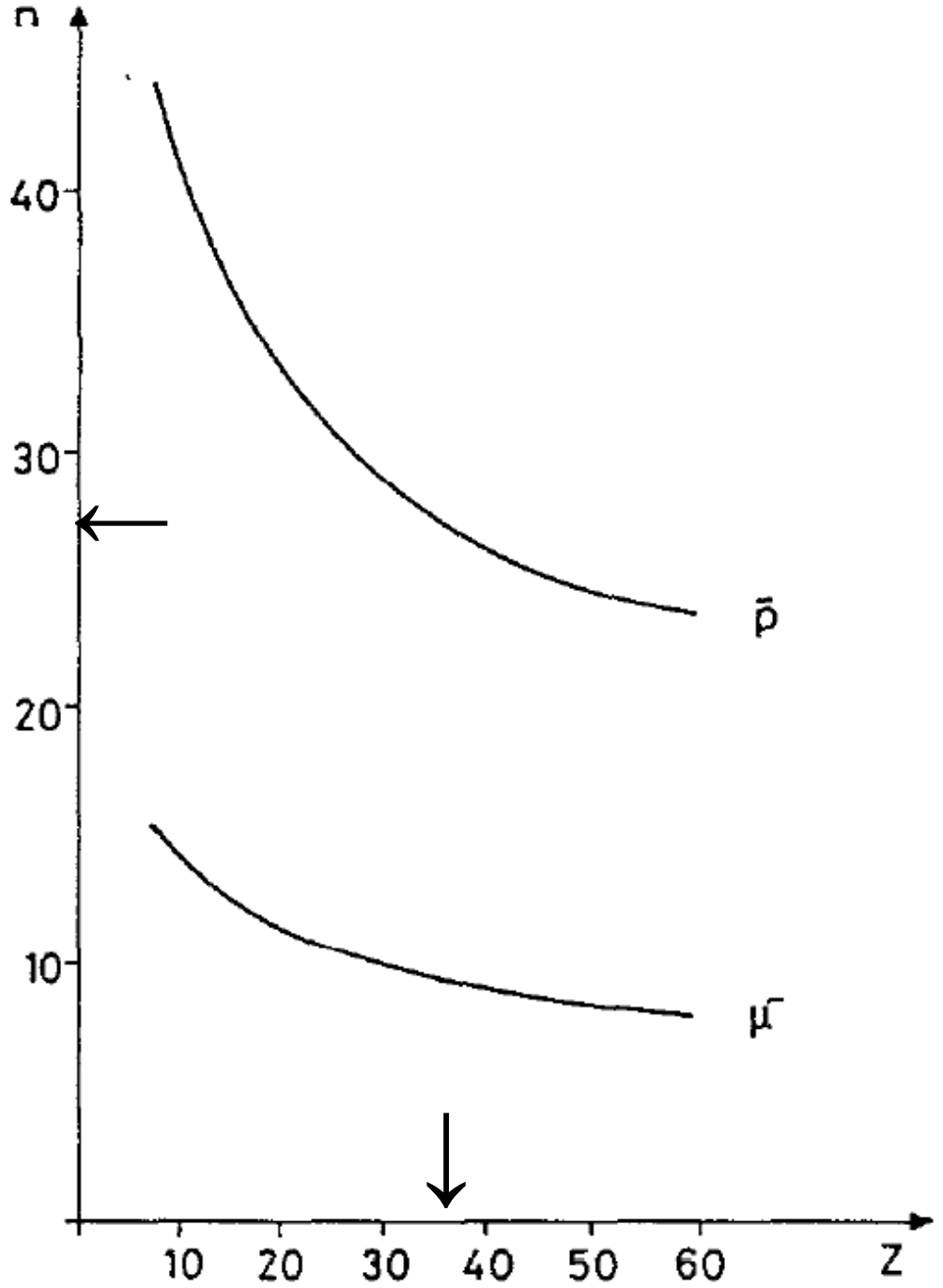

L. Simoms et al, NIM, B87, 293 (1994).

PS175: Precision experiments and analyses of Anti-protonic X-ray spectroscopy:

- Noble gases; Ar, Kr, Xe
- Electronic K, L energy regions
- MCDF atomic energy determination
- Ferrell's formula of Γ_A and Γ_X

→ Analysis of X-ray intensity at these energy regions,

providing the information of Auger electrons. .

Is fully quantitative analyses of X-ray intensities in these energy regions feasible by improving Farrell's formula, possibly leading to understanding dynamics of atomic cascade in electron cloud?

e.g. A. Altman, Z. Fried, *Phys. Rev*. **A28**, 455 (1983).

5. Prospects in the physics of anti-protonic atoms

More informative data and analyses of :

a) Energies and intensities of X-ray spectra in both energy regions of atomic cascade and nuclear absorption, and

b) Pion emission from nuclear absorption (PUMA)

⟶ in wider range of atoms and nuclei, than those restricted by shifts-widths observation:

Thus a) is important for b) and for future investigations of anti-protonic atoms.

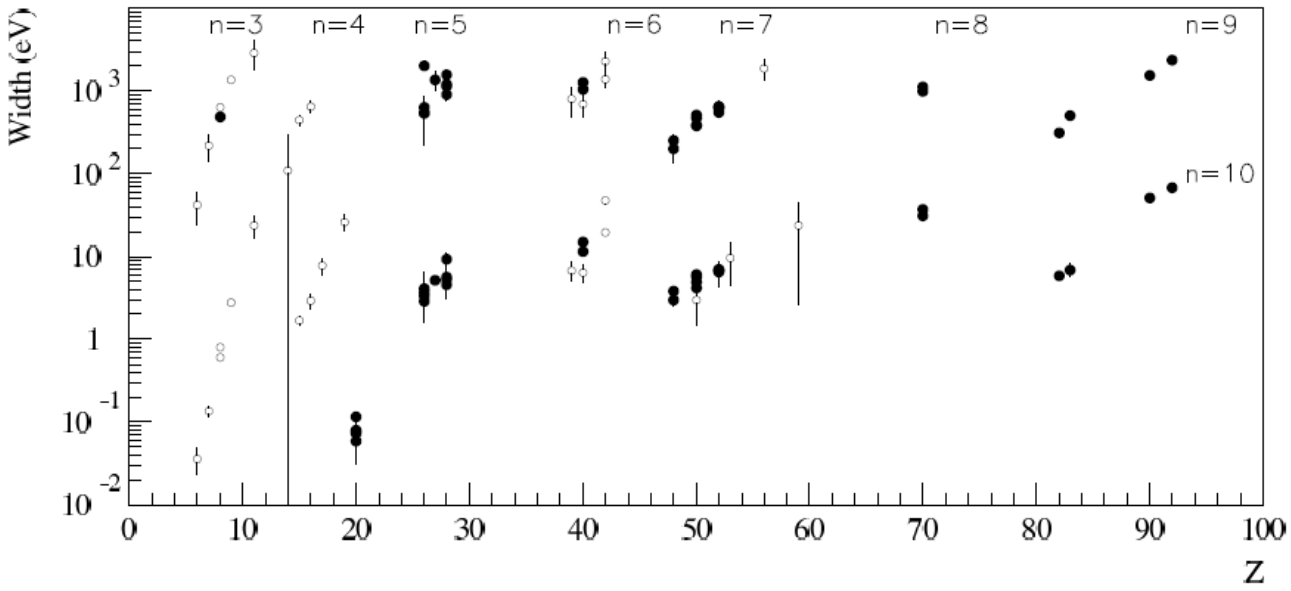

PS209, ibid.